CHARLES UNIVERSITY IN PRAGUE

Faculty of Pharmacy in Hradec Králové

Department of Pharmacology and Toxicology

COMPARISON OF RADIOLABELLED FATTY ACID (^{18}F-FTHA) AND ^{18}F-FDG IN IMAGING OF BROWN ADIPOSE TISSUE

Maastricht University

Department of Nuclear Medicine

Netherlands

Rigorous thesis

Thesis supervisor: Dr. Matthias Bauwens

Thesis consultant: PharmDr. Jana Ramos Mandíková, Ph.D.

Hradec Králové 2016 Mgr. Tereza Vašků

„Hereby I declare that this thesis is my original copyright work. All sources and data I used indirectly or from other sources are characterized with list of sources. The diploma thesis has not been submitted for other or identical academic degree."

„Prohlašuji, že tato práce je mým původním autorským dílem. Veškerá literatura a další zdroje, ze kterých jsem při zpracovávání čerpala, jsou uvedené v seznamu použité literatury práce. Práce nebyla použita k získání jiného či stejného titulu."

V Hradci Králové 2016

Acknowledgements

At the first, I would like to thank patient Dr. Matthias Bauwens, my supervisor in Netherlands, who helped and guided me throughout the whole project.

I also thank Prof Felix Mottaghy, the director of Department of Nuclear Medicine, for accepting me in the institute.

Next my thanks belong to my Czech consultant PharmDr. Jana Ramos Mandíková, Ph.D. for her valuable remarks and advice during this work.

Lastly, I would like to thank to my family for their support of my stay in Netherlands.

Charles University in Prague
Faculty of Pharmacy in Hradec Králové, Department of Pharmacology and Toxicology
Student: Mgr. Tereza Vašků
Supervisor: Dr. Matthias Bauwens: Maastricht University, Netherlands
Consultant: PharmDr. Jana Ramos Mandíková, PhD
Title of diploma thesis: Comparison of radiolabelled fatty acid (^{18}F-FTHA) and ^{18}F-FDG in imaging of brown adipose tissue

Brown adipose tissue (BAT) is highly metabolically active tissue, which consumes glucose and free fatty acids (FFA) during the process called thermogenesis. Due to these characteristic features, it is possible to quantify the activity of the BAT by non-invasive imaging methods (by using radiopharmaceuticals). Nowadays, one of the most frequently used substances is the radiopharmaceutical called ^{18}F-FDG (radiolabelled glucose by fluoride). The ^{18}F-FDG is in clinical practice used for metabolically active tissues diagnosis, notably tumours. We focused in this study on synthesis of radiolabelled fatty acid, namely on the radiopharmaceutical 14(R,S)-[^{18}F]Fluoro-6-thia-heptadecanoic acid (^{18}F-FTHA). Fluor-labelled fatty acid is used notably for myocardial metabolism observation. The goal of the thesis was a synthesis of radiopharmaceutical ^{18}F-FTHA using a semimanual module in an environment of sufficient purity and yield. Consequently, the goal was to reach molecular imaging of iBAT in case of a model of a mouse using two particular radiopharmaceuticals, ^{18}F-FDG and ^{18}F-FTHA. We tried to answer the question whether there is a link between radiopharmaceutical uptake and surrounding temperature and whether feeding with various nutrition has an impact on metabolism activity iBAT. After the detection of these radiopharmaceuticals we used μPET scanning and the scan was consequently assessed, using the PMOD™ module. We succeeded to synthetize the radiopharmaceutical ^{18}F-FTHA in the sufficient yield (≥ 55 %) and in the sufficient purity (≥ 94 %). Thanks to the results of this study, we can claim high uptake of the radiopharmaceutical ^{18}F-FDG when there is an exposure of an organism to cold and when aliment with low rate of fat and glucose is served. In case of the radiopharmaceutical ^{18}F-FTHA is the uptake significantly lower and there was no relation to the temperature and nutritional conditions detected. We have reached the conclusion that better visualisation of iBAT provides the radiopharmaceutical ^{18}F-FDG.

Univerzita Karlova v Praze
Farmaceutická fakulta v Hradci Králové, Katedra farmakologie a toxikologie
Student: Mrg. Tereza Vašků
Školitel: Dr. Matthias Bauwens: Maastricht University, Netherlands
Konzultant: PharmDr. Jana Ramos Mandíková, PhD.
Téma diplomové práce: Srovnání radioaktivně značené mastné kyseliny (^{18}F-FTHA) a ^{18}F-FDG v zobrazování hnědé tukové tkáně.

Hnědá tuková tkáň (BAT) je vysoce metabolicky aktivní tkáň, která k procesu zvanému termogeneze, spotřebovává glukózu a volné mastné kyseliny. Díky těmto vlastnostem je možné aktivitu BAT kvantifikovat neinvazivními zobrazovacími metodami pomocí radiofarmaka. Jednou, v dnešní době velmi široce užívanou látkou, je radiofarmakum ^{18}F-FDG (fluorem značená glukóza). ^{18}F-FDG se používá v klinické praxi pro diagnostiku metabolicky aktivních tkání, zejména nádorů. V této studii jsme se zaměřili na syntézu radioaktivně značené mastné kyseliny a to konkrétně na radiofarmakum 14(R,S)-[^{18}F]Fluoro-6-thia-heptadecanovou kyselinu (^{18}F-FTHA). Fluorem značená mastná kyselina je využívána zejména ke sledování metabolismu myokardu. Cílem této práce byla syntéza radiofarmaka ^{18}F-FTHA semimanuálním modulem v dostatečné čistotě a výtěžku a následně molekulárně zobrazit iBAT u modelu myši pomocí dvou radiofarmak ^{18}F-FDG and ^{18}F-FTHA. Pokusili jsme se odpovědět na otázku, zda existuje závislost vychytávání radiofarmaka na okolní teplotě a zda nutričně rozdílné krmení, dokáže ovlivnit na metabolickou aktivitu iBAT. Pro detekci těchto radiofarmak jsme použili μPET snímání a následně byl snímek vyhodnocen PMOD™ modulem. Podařilo se nám nesyntetizovat radiofarmakum ^{18}F-FTHA v dostatečném výtěžku (≥ 55 %) a čistotě (≥ 94 %). Díky výsledkům této studie můžeme tvrdit, že vychytávání radiofarmaka ^{18}F-FDG je nejvyšší při působení chladu na organismus a zároveň pokud je podávána potrava s nízkým obsahem tuku a glukózy. V případě radiofarmaka ^{18}F-FTHA je vychytávání signifikantně nižší a nedetekujeme zde vztah k teplotním či nutričním podmínkám. Došli jsme k závěru, že lepší vizualizace iBAT jsme dosáhli radiofarmakem ^{18}F-FDG.

Content

1. Abbreviation list

123I-BMIPP	**β-methyl-p-123I- Iodophenyl-Pentadecanoic Acid**
^{18}F-FDG	**18F flourodeoxyglucose**
aBAT	**Axiliary brown adipose tissue**
Acetyl-CoA	**Acetyl-Coenzyme A**
ATP	**Adenosine triphosphate**
BAT	**Brown adipose tissue**
BMHDA	**β-methyl[1-^{11}C]heptadecanoic acid**
cAMP	**Cyclic adenosinmonofosfat**
CD36	**Cluster of differentiation glucose transporters**
CH_3CN	**Acetonitrile**
CT	**Computer tomography**
DEC- UM	**Dier experimenten Commisie - Maastricht University**
EtOAc	**Ethyl acetate**
FAD	**Flavin adenine dinucleotide**
$FADH_2$	**Flavin adenine dinucleotide-hydroquinone form**
FAO	**Fatty acid oxidaton**
FAT/CD36	**Fatty acid translocase CD36**
FATP	**Fatty acid transport protein**

FFA	**Free fatty acids**
FTHA	**14(R,S)-[^{18}F]Fluoro-6-thia-heptadecanoic acid**
FTO	**18-[^{18}F]-fluoro-4-thia-oleate**
FTP	**[^{18}F]Fluortriopride**
H218O	**Water(oxygen-18)**
HCl	**Hydrochloric acid**
HPLC	**High-performance liquid chromatography**
HU	**Hounsfield unit**
i.p.	**Intraperitoneal injection**
i.v.	**Intravenous injection**
iBAT	**Interscapular brown adipose tissue**
IPPA	**^{123}I-phenyl-pentadecanoic acid**
KOH	**KOH**
LCFA	**Long chain fatty acids**
LPL	**Lipoprotein lipase**
MIBG	**^{123}I- Metaiodobenzylguanidin**
MVO2	**Mixed Venous Oxygen Saturation**
NAD	**Nikotinamidadenindinukleotid**
PET	**Positron emission tomography**
RNL	**RadioNucliden Laboratorium**

SPECT	**Single photon-emission computed tomography**
SUV	**Standardized uptake volume**
TAG	**Triacylglyceride**
THF-α	**Tumor necrosis factor alpha**
TLC	**Thin-layer chromatography**
UCP	**Uncoupling protein**
WAT	**White adipose tissue**
µPET	**Micro positron emission tomography**

2. Introduction

Brown adipose tissue (BAT) is known for the unique function which is transfer an energy from food into heat. It has an irreplaceable function in new-borns, because it provides them thermal stability. In the previous diploma thesis I focused on describing the roles of BAT such as the most frequent location in humans and in mouse model. I tried to explain and describe unique function of uncoupling protein one (UCP1) to produce heat and provides thermal stability to new-borns. In previous thesis there were detailed described endocrine functions and mediators which has an influence to brown fat. I wrote about possibility to detect and measure thermogenesis such as a process where the energy is transferred to the heat and this step is possible to detect and measure due to modern positron emission tomography (PET). I would like to make a reference to diploma thesis with title Molecular imaging brown adipose tissue in mice in case of detailed description of brown adipose tissue.

In following part I would like to aim at more detailed on possibility to detect BAT via radiolabelled fatty acids especially 14(R,S)-[^{18}F]Fluoro-6-thia-heptadecanoic acid (^{18}F-FTHA) and compare with previous data from commonly used radiotracer fluorodeoxyglucose (^{18}F-FDG). I will describe the mechanism of synthesis of radiolabelling fatty acid. The radiotracer ^{18}F-FTHA is commonly used for myocardium imaging which is incorporated to high active tissues (Renstorm et al., 1998) and we suspect that we will be able to visualise BAT by radiotracer ^{18}F-FTHA as well.

During the whole project it was tried to keep the main and important questions. What is the function of BAT in the body of an adult? Under what conditions is BAT active and is it possible to generate heat and through it reduce fat deposits thanks to the ability of this tissue? If we would like to have a correct answers and be sure that how this depots works we have to take the single knowledge from particular fields and construct the correct hypothesis. From point of view nuclear medicine at the moment we are working on the part how we are able to best visualize BAT and if the surrounding conditions have effect to metabolic activity.

3. Theoretical part

3.1. Brown adipose tissue

I would like to highlight the most important knowledge about brown fat and mention few finding which we already have from different part of science. This necessary knowledge allow us to answer to many questions and set up other hypothesis.

The brown adipose tissue has a main function called thermogenesis (production of heat). It is also able to store fats in TAG form and also can have an influence to the whole body via various mediators (Wu Z et al., 2012).BAT is highly vascularized and richly innervated by terminal fibers of the postganglionic neurons of the sympathetic nervous system. It produces around hundred chemical compounds, which play an important role in metabolic regulations, direction of food intake, inflammation and other processes such as leptin, resistin, cytokine, tumour necrosis factors (THF-α), interleukin-6 (IL-6) and others (Halvorson and al., 1990). We can detect two main type of adipose tissue which have a difference functions. White adipose tissue (WAT) stores energy in lipid pool while brown adipose tissue (BAT) uses substrates for production of body heat. They have a different location of depots, morphology and functions (Ahima et al., 2000).We can divide them according to amount of mitochondria. The BAT has much higher amour of mitochondria than in WAT has (Shu-Xin Z, 1999).

The Swiss physician Conrad Gessner as first in 1551 detected BAT in hibernating marmots (Tews, 2011). Originally it was believed that the amount of BAT was fractional or completely disappear in adult humans. During the last 10 years, BAT has received considerable attention in the field of nuclear medicine. BAT has been proven to accumulate ^{18}F-fluorodeoxyglucose (^{18}F-FDG) and other radiotracers (Wolfgang at al., 2004). In the modern we are encountering with rise of obesity and metabolic decease. Due to this issues the researches for whole over the world try to find the effective way how to reduce risk of metabolic disease or decrease human weight. Nowadays we are looking at the brown depots as the possible antiobesity organ which could regulates the homeostatic nutrient processes (Cypess et al., 2009).

3.2. Lipids as source of energy

The lipids utilization we can simply summarized into three steps. First, mobilization of lipids – hydrolysis triacylglycerides (TAG) into fatty acids and glycerol and their transport to blood. Second, activation of FAs into cytosol and their transport to mitochondrial matrix. The last step is process of β-oxidation which is able to fatty acids (FAs) degradation into acetyl-CoA. Acetyl-CoA enters to Krebs cycle or it creates keto acids (Marchington et al., 1990).

In order to corporation of FAs into cell they have to overcome a cell membrane. There are few mechanisms how to FAs go through to cytosol. It depends to the length, FAs with short chain (to 12 C) can go through by passive diffusion. The FAs with longer chain use the various transport system such as FATP (fatty acid transport protein) or FAT/CD36 (fatty acid translocase) (Boenen et al., 2004). Fatty acids must be activated before they can be carried into mitochondria, where fatty acid oxidation occurs (Figure 1). This process occurs in two steps by the enzyme fatty acyl-CoA sythetase (fatty acid thiokinase). Subsequently Acyl- CoA can transverse to mitochondrial matrix. There is also depends on length of chain. The Chain up to 10 carbons can go through by simple diffusion, the moderate chains with 12 to 18 carbons need for transfer carnitine carrier. The long chain of fatty acids above 18 carbons ca not incorporate to matrix (Hoppel et al., 2003).

β-oxidation of fatty acids occurs via four recurring steps which first is dehydrogenation by FAD. LCFA is dehydrogenated to create a trans double bound between C2 and C3. This is catalysed by acyl CoA dehydrogenase to produce trans-delta 2-enoyl CoA. It uses FAD as an electron acceptor and it is reduced to FADH2. Second step is hydration. The bond between C2 and C3 (the reaction is stereospecific, forming only the L isomer). Third steps is the oxidation of L-beta-hydroxyacyl CoA by NAD+. This converts the hydroxyl group into a keto group. The last steps is the cleavage of beta-ketoacyl CoA by the thiol group of another molecule of Coenzyme A. The thiol is inserted between C2 and C3. Acetyl-CoA, water and 5 ATP molecules are the other products of

each β-oxidative event, until the entire acyl-CoA molecule has been reduced to a set of acetyl-CoA molecules (Fillmore et al., 2011).

Fatty acids are oxidized by most of the tissues in the body. However, some tissues such as the red blood cells (which do not contain mitochondria) and cells of the central nervous system (fatty acids cannot cross the blood brain barrier) use as source of energy carbohydrates (Berg et al., 2002)

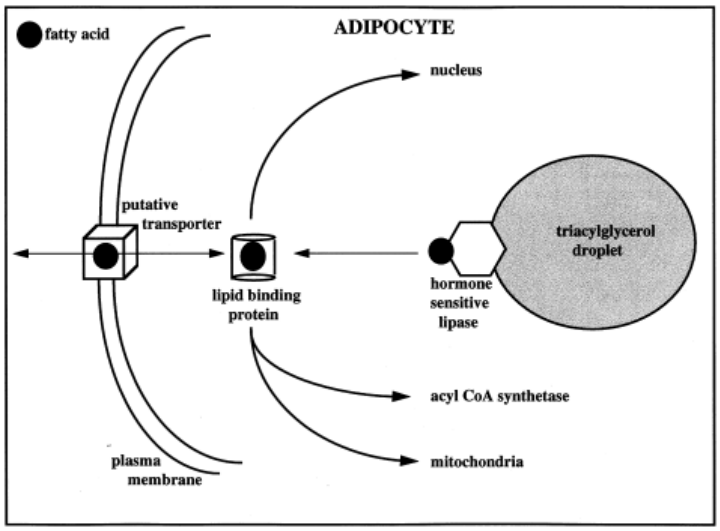

Fig 1: FAs pathways in adipocytes. Lipid-binding proteins bind intracellular fatty acids and may aid in fatty acid transport to cellular locales such as the nucleus or mitochondria and/or to enzyme partners acetyl-CoA synthetase (Bernlohr et al., 1999).

3.2.1. Incorporation of fatty acids to iBAT

The ability of adipose tissue to efficiently up take of long chain fatty acid is the key to their physiological functions in energy storage and thermogenesis respectively. Fatty acid (FA) uptake by adipocytes plays an important role in the maintain lipid homeostasis (Eberlé et al., 2004). Adipose tissue produces lipoprotein lipase which can generate FAs in the local vasculature through its action on TAG rich lipoprotein particles. FAs transition across the endothelin cell layer and then bound intestinal albumin in blood

stream (Hagberg et al., 2010). The actual mechanism of transmembrane fatty acid flux is controversial. Fatty acid may enter fat cells by means of diffusional fatty acid flip-flop or with the aid of one or more plasma membrane transport proteins. FAs or their metabolites have a multifactorial role in adipose tissue such as transcriptional control, membrane synthesis, regulators of cellular metabolism and energy storage in the triglyceride droplet. (Bernlohr et all, 1999).

Triglyceride-rich lipoproteins transport lipids in blood stream. Due to cold exposure, the clearance of triglycerides is drastically accelerated as result of increased uptake in BAT trough incorporated transmembrane receptor CD36 (cluster of differentiation) (Bartelt et al., 2011). This scavenger receptor can recognize a negative charge and remove modified lipoproteins. The recent report shows that receptor CD36 also uptakes coenzyme Q which is an essential component of the mitochondrial electron transport chain and is required for normal BAT function (Anderson et al., 2015). Otherwise, the following mechanism of incorporation of lipids to lipid pool is one of the unsolved questions. The lipids may have direct influence on UPC1 or they may be incorporated to lipid pool. It undergoes further research, whose factors play key role in a correct pathway determination (Chaves et al., 2008).

In cell of BAT, FAs can be either synthesized de novo or they are imported from circulation. We can consider FAs as the main fuel for heat generation but the whole mechanism of FAs uptake and its regulation has remained unclear. Nevertheless, the fatty acid transport protein was detected on the plasma membrane of BAT and upregulated in response to cold stimuli with an increase in the rate of fatty acid uptake (Taruel et al., 2000). Therefore, this is important to maintain adequate stocks of triglyceride for normal function of BAT. One of these mechanisms is lipolysis of intracellular lipid droplets driven by hormone-sensitive lipase and adipose triglyceride lipase. The other ones are through the localised hydrolysis of lipoproteins by lipoprotein lipase (Taruel et al., 2000).

3.3. Radiolabelled fatty acid

The interest in myocardial energy metabolism, visualisation and quantification has progressed into development of new radiopharmaceutical agents. The radiotracer ^{18}F-FDG which is commonly used is just reflecting glucose metabolism but it cannot provide information about myocardial oxygen consumption (MVO2) or fatty acid metabolism (Bergmann et al., 2001). The studies in cardiac metabolism focuse on the characterisation of myocardial kinetic of the long chain fatty acid. Currently, ^{11}C-palmitate is the preferred method of measuring MVO2 and for reflection fatty acid metabolism noninvasively (Runkle et al., 2011). Acetate is a two-carbon chain free fatty acid whose primary metabolic fate is rapidly conversion to acetyl–CoA and metabolism through the tricarboxylic acid cycle. Because of the close coupling between the tricarboxylic acid cycle and oxidative phosphorylation, myocardial turnover of 11C-acetate reflects overall oxidative metabolism or MVO2. However, this approach suffers from several disadvantages including reduced images quality and specificity and the need for an onsite cyclotron and radiopharmaceutical production capability (Y Li et al., 2015).

In process of developing a functional fatty acid radiotracer with high uptake in energy consumption tissue, there were a few experiments of substitution. Omega-^{18}F-Fluoro LCFA analogues have myocardial uptake and clearance rates similar to radiolabelled palmitate. 6 and 7-(^{18}F)Fluoropalmitate also showed uptake and clearance from heart similar to palmitate but fluorine substitution at the alpha-carbon of stearic acid caused a large decrease in myocardial uptake. The other advantage was the longer half-life of ^{18}F in comparison to 11C. It allows longer PET measurement periods and off-site production of radiotracers. However, the straight chain (^{18}F)Fluoro fatty acids appears to offer no further advantage over palmitate (Z Tu et al., 2010).

The β-methyl substituted analogue of palmitate [1-11C] heptadecanoic acid (BMHDA) has been proposed to provide a longer retention as a consequence of inhibited β-oxidation (Takeyama et al., 1995). The following studies with fluorine isotope and with substitution with 3-methyl and 5-methyl of (^{18}F)-fluoro palmitate analogues showed longer retention than nonsubstitued palmitate. However, the maximal uptakes of the

branches-chain ^{18}F-labelled LCFA analogues were lower than for the straight chain analogue, suggesting a steric effect on initial steps of transport and metabolism. Also high uptake of radioactivity in bone indicated defluorination of both methyl-substitued LCFA analogues (Peterson et al., 2010).

This fatty acid analogues have recently received interest as false substances and inhibitors of fatty acid metabolism. They are accepted for many processes of LCFA metabolism but complete β-oxidation of the chain is blocked by the sulfur heteroatom. This sulfur (thioether) decreases the hydrophobicity of the chain significantly but (Berge et al., 2002).

3.3.1. 14(R,S)-[^{18}F]Fluoro-6-thia-heptadecanoic acid (^{18}F-FTHA)

The non-invasive assessment of regional myocardial oxidative metabolism by PET has been recently forwarded with the use of úl-11C]acetate. Although β-oxidation of LCFAs represents the major source of mitochondrial acetyl-CoA in normal conditions, the profile of substrate utilization is sensitive to nutritive metabolic and pathologic alterations.^{18}F-FTHA is a radiolabelled long-chain fatty acid (LCFA) analogue designed to undergo metabolic trapping subsequent to its commitment to the β-oxidation pathway. (G Hao et al., 2015). The half-life of ^{18}F (110 minutes) allows for regional distribution of probes, while the presence of the sulfur heteroatom blocks the β-oxidation of the fatty acid and also renders the molecule as a poor substrate for incorporation into complex lipids. Most of the fatty acids tracers for PET imaging have been designed to reflect myocardial β-oxidation. ^{18}F-FTHA was one of the first radiotracers developed using this approach. Initial results were promising with uptake and retention in the myocardium accordingly with changes in substrate delivery, blood flow and workload in animal models (Gropler et al., 2010). Moreover, PET with ^{18}F-FTHA was used to evaluate the effects of various diseases such as coronary artery disease and cardiomyopathy on

myocardial fatty acid metabolism. However, uptake and retention of ^{18}F-FTHA has been shown to be insensitive to the inhibition of β-oxidation by hypoxia reducing enthusiasm for this radiotracer to measure myocardial metabolism (Dilsizian and Pohost, 2011).

3.3.2. Synthesis Procedure

The scientist Timothy R. DeGrado from Institute in Julich, Germany as first published the synthesis of ^{18}F-FTHA in 1991. He described this synthesis as the nucleophilic radiofluorination of benzyl-14-(R,S)-tosyloxy-6-thia-heptadecanoate in acetonitrile utilized (Kryptrofix 2.2.2/K)CO2 for anion activation. The resulting (^{18}F)fluoro-ester was quantitatively hydrolysed with addition of aqueous KOH and the product purified by reversed phase HPLC (Figure 2) (DeGrado et al., 1991).

Summary of sythesis

- **Fluorination**

The ^{18}F-FTHA is prepared by direct fluorination of Benzyl-14-tosyloxy-6-thia-heptadecanoate (disolvation in CH_3CN) to an azeotropic dried mixture Kryptofix 2.2.2. Kryprofix is 4,7,13,16,21,24-Hexaoxa-1,10-diazabicyclo[8.8.8]hexacosane Figure 1. This compound is used extensively as a phase-transfer target which allows the trapping fluoride from the radioactive water (Moerlein et al., 1989). However it has considerable acute toxicity and it must be remove from the solution of ^{18}F-FTHA. Separation of the fluorine-19 compound is performed by silica gel chromatography on glass (Y Lao et al., 2012).

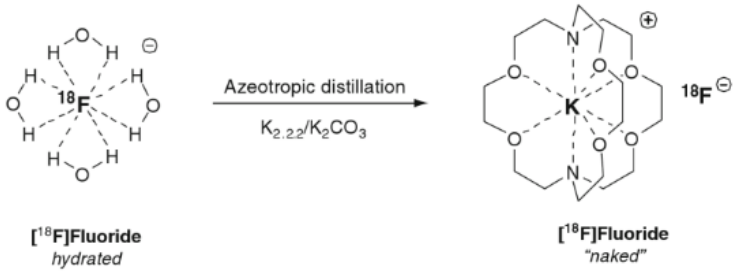

Fig. 1: The mechanism of (^{18}F)fluoride activation. The ^{18}F is removed from water in exchange with Kryptofix/potassium carmobate system (Moerlein at al., 1989).

Compound benzyl-14-(R,S)-tosyloxy-6-thia-heptadecanoate has two active sites which are susceptible to nucleophilic attack (Figure 2). Higher temperature and an excess of base lead to hydrolysis of the ester functional group. Heating the reaction mixture up to 90 °C increased the yield. On the other hand the further heating of the reaction mixture reduced the yield of synthesis due to decomposition or ester cleavage of precursor and product (DeGrado et al., 1991).

- **Hydrolysis**

This step has a crucial value in the production. In case of incomplete hydrolysis, the residues of un-hydrolyses ester remains in the sample. It cannot be removed by solid phase extraction from the final sample and can cased higher uptake ratios in the liver. It must be strictly kept the time of heating (90-95 °C for 5-8 min) and the product will be obtained in acceptable purity (less than 10 % un-hydrolysed compound) (DeGrando et al, 2010).

First step: Preparation of ^{18}F-potassium fluoride

Anion Fluorine-18 is prepared by 18 MeV proton bombardment of an enriched $H_2{}^{18}O$ sample in cyclotrone and subsequently the sample is held in a gold-coated silver target. After recovery of $H_2{}^{18}O$ over an anion exchange resin. This ion exchange polymer which has a typically porous and high surface area. The trapping of ions occurs with the accompanying releasing of other ions. The fluorine-18 anion is eluted by a 1 % potassium carbone solution. The eluted solution was directly used in the labelling process. (Baum, 2013).

Second step: Preparation of 6-thia-14-fluoro-heptadecanoic acid

Anhydrous acetonitrile is added to a vial containg solid potassium fluoride and solid Kryptofix 2.2.2. These mixture is azeotropically dried two times by the addition of anhydrous acetonitrile portions. The vial was cooled and a solution of benzyl-14-(R,S)-tosyloxy-6-thia-heptadecanoatein anhydridous nitrile is add to the dried mixture. The vial is heated to 80 °C for 8 min. The TLC control of the reaction mixture using two solvent systems diethyl ether and ethyl acetate: hexane (1:3 v/v) demonstrated the completion of the reaction. The mixture is cooling and dissolved in diethyl ether and passed through two Sep-Pec^{TM} columns (Baum, 2013). This column helps to separate mixture by solid nonpolar material. The organic layer is dried over anhydridous sodium sulphate and purified by silica gel on glass using a mixture hexane:EtOAc as the mobile phase. The fluoride compound is separated while the starting material migrated to the column (Southan, 1987). The intermediate product benzyl-14-(R,S)-(^{18}F)fluor-6-thia-heptadecanoat (Figure 2) is transferred to a conical borosilicate vial containg potassium hydroxide solution and the reaction mixture is heated to 95 °C for 3 min and subsequently cooled to room temperature followed by neutralization using HCl. During the all steps the mixture is bubbling using a flow nitrogene (DeGrado et al., 2010).

HPLC is used in order to investigate the purity of the final product. The average of radiochemical purity is detected around 91 % +-3 % and yield of ^{18}F-FTH the reaction is

around 74 GBq (according to experiments by Amir R. Jalilian et al., 2006). The whole process of synthesis takes less than 20 min.

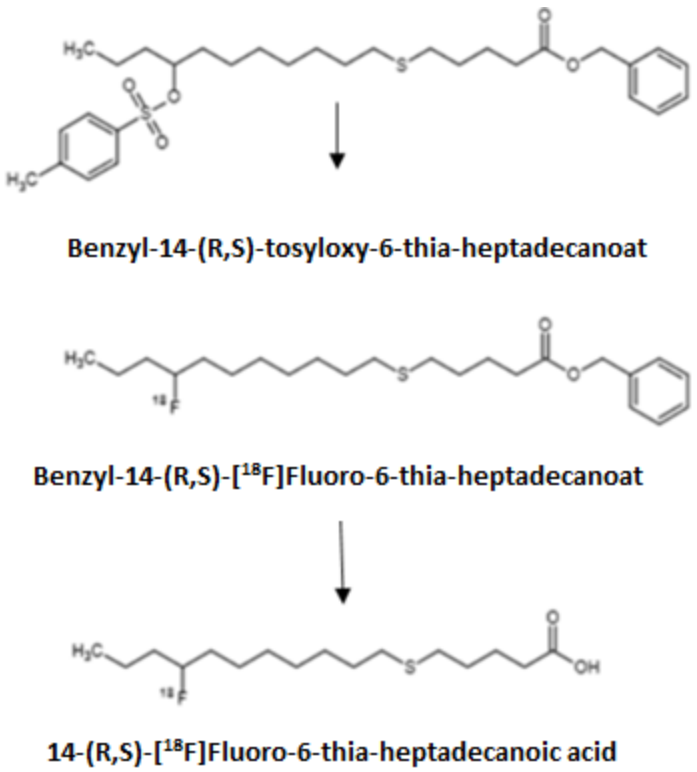

Fig. 2: Mechanism of synthesis 18F-FTHA. Nucleophilic radiofluorination of precursor benzyl-14-(R,S)-[18F]tosyloxy-6-thia-heptadecanoat and hydrolysis of ester benzyl-14-(R,S)-[18F]Fluoro-6-thia-heptadecanoat by aqueous KOH (Baum, 2013).

3.3.3. Fluorine radiolabelled fatty acids analogues

^{11}C-labelled fatty acid PET radiotracers have been in use for over 35 years but have been mainly confined to research studies due to theirs short physical half-life (20.4. m). However. ^{11}C-labelled fatty acid probes have value to indicate accumulation of exogenous fatty acids in the myocardial TAG pool. This tracer is characterized by a slow turnover. (Geltman at al., 1994).

^{18}F-FTHA was the first generation thia fatty acid probe synthetized in 1990. Due to big advantage such as high myocardial uptake, longer retention and rapid clearance from the bloodstream is the most investigated thia fatty acid. ^{18}F-FTHA has been used as a fatty acid uptake probe in human studies in heart, liver, skeletal muscle and brain. Nevertheless, the lack sensitivity to lower FAO rates in hypoxic myocardium motivated further tracer development to improve specificity to monitor FAO rates (Pandey et al., 2011).

16-[^{18}F] fluoro-4-thia-palmitate (FTP)

The second generation of thia fatty acid analogue (palmitate-based analogue) were synthetized in 2000. Being already mentioned, ^{18}F-FTHA has shown the inhibition β-oxidation by hypoxia. This problem was solved by developing 16-^{18}F-fluoro-4-thia-palmitate (FTP). This modification retains the metabolic trapping function of the radiotracer which is proportional to fatty acid oxidation under normal oxygenation and hypoxic conditions. FTP is currently undergoing commercialization as it enters early Phase 1 evaluation (Gropler et al., 2010). The other modification of 6-thia fatty acid analogue 17-(^{18}F)Fluoro-6-heptadecanoate was insensitive to the decrease in palmitate oxidation rate in hypoxic hearts. Thus, the placement of the thia substituent at the fourth position significantly improved the specificity for indication of FAO (Pandey and al., 2011).

18-[^{18}F] fluoro-4-thia-oleate (FTO)

Abnormalities of fatty acid oxidation are associated with several cardiovascular diseases and diabetes. FTO was recently prepared and described in 2010. It was evaluated in relationship to the previously developed ^{18}F-FTP. Results of biodistribution and small-animal PET studies of FTO were compared with those for the previously developed ^{18}F-

FTP, showing enhanced myocardial imaging characteristics and increased specificity for evaluation of FAO rates *in vivo* (DeGrado et al. 2010).

3.3.4. Possibility of iBAT imaging in other radiotracers

PET tracers used in studies of BAT with quantitative modelling are summarized in Table 1. BAT has also been detected using MRI, 99mTechnetium(Tc)-sestamibi, and 123I-metaiodobenzylguanidine single-photon emission computed tomography/computed tomography (MIBG SPECT/CT) (Goetze et al., 2008).

Tab 1: PET tracers for iBAT quantitative evaluation.

	TRACER	**HALF-LIFE (MIN)**
PERFUSION	$[^{15}O]H_2O$	2
GLUCOSE UPTAKE	$[^{18}F]FDG$	109
FREE FATTY AID METABOLISM	$[^{18}F]FTHA$	109
	$[^{11}C]$acetate	20
OXIDATIVE METABOLISM	$[^{15}O]O_2$	2
	$[^{11}C]$acetate	20

4. Aim of thesis

1 The stated goal of this thesis is radiolabelling of fatty acid by 18 fluoride and optimization of labelling processes using semimanual machine in university hospital Rheinisch-Westfälische Technische Hochschule in Aachen. Another object is try to get sufficient quality of radiotracer ^{18}F-FTHA such as purity and high activity for creating an image of brown adipose tissue through μPET scan.

2 The final object of the thesis is comparison of two radiotracers ^{18}F-FDG and ^{18}F-FTHA and try to answer two main questions. First, which of these two radiotracers is more suitable for the imaging of interscapular brown adipose tissue? Second, is there any relation between the surrounding temperature and type of nutrition to uptake in interscapular brown fat? In order to get this answers use the previously optimized procedures for μPET scan, PMOD^{TM} module and subsequently statistically compare the SUV values. The goal of the thesis is to determine the radiotracer with better resolution, quality of images and highest uptake in interscapular brown adipose tissue.

5. Experimental part

For this project the similar Material and Methods (described in previous diploma thesis) were used (Vašků 2015). It was requited to strictly abide the conditions of housing animals, processes of manipulation, procedure of application radiotracers and evaluation of final images. Due to maintenance of this methods which were set up at the beginning of this project we were able to make qualified evaluation and comparison between two radiotracers ^{18}F-FDG and ^{18}F-FTHA.

5.1. Materials

5.1.1. Experimental animals

Six weeks old mice model (type C57/BIJ6, male, black, registered farming) were kept in accordance with the National Institute of Health Guide for Care and Use of Laboratory Animals. These whole research were submitted to Animal Experiments Committee – Dier experimenten Commisie in Maastricht University, DEC – UM and subsequently were approved. A license has been issued by the Centrale Commissie Dierproven (CCD), Netherlands.

All animals were obtained from commercial laboratory animal facility Harlan, Netherlands. The initial weight of mice was approximately in range 20-23 g.

5.1.2. Chemicals

- Radiopharmaceutical: ^{18}F-FDG, GE Healthcare Radiopharmaca Apotheek, Eindhoven, Netherlands
- Isoflurane: IsoFlo, Abbott, USA
- Pentobarbital: Abbott, USA

Chemicals for synthesis of ^{18}F-FTHA:

- Isotope: ^{18}F was generated via cyclotron in department of Nuclear Medicine, RWTH, Aachen, Germany
- Kryptofix 222 (10-DIAZABICYCLO[8.8.8]HEXACOSANE), Merck KGaA, Darmstadt, Germany
- Acetonitrile for DNA synthesis max. 10 ppm Water, Merck KGaA, Germany
- Argon: Linde, Germany
- Precursor: Benzyl-14-(R,S)-tosyloxy-6-thia-heptadecanoate: ABX, Dresden, Germany
- Dichlormethan: VWR, Darmstadt, Germany
- Dimethylformamid: Sigma Aldrich, Germany
- Dimethylsulfoxid: Acros Organics, Germany
- Acetic Acid: Merc KGaA, Germany
- Ethyl Acetat: AppliChem, Germany
- Ethylmethylketon: Merck KGaA, Germany
- [^{18}F]-target Wather: Eckert & Ziegler GmbH und Uniklinikum Aachen
- Kalciumcarbonate: Merck KGaA, Germany
- Methanol: LiChrosolv Methanol for Chromathogryphy (99.8 %), Merck KGaA, Germany
- Natriumhydrogencarbonate: Merck KGaA, Germany
- Tetrahydrofurane: Roth, Germany
- Toluol: Merk KGaA, Germany
- Wather: LiChrosolvl Water for Chromatography (99.8 %), Merck KGaA

5.1.3. Machines

- **MICROPET FOCUS 120®** Siemens Medical Solutions, Inc (formerly) Concorde Microsystems, Inc, Knoxville, TN.

Detector material: Lutetium oxyortho-silicate (LSO). Timing resolution: 3 nsec, Peak noice equivalent count (NEC) rate was measured as 580 kilo counts per second (kcps). Data acquisition: Manager 2.4.1.1. Reconstruction algorithm: filtered back projection (FBP), ordered subset expectation maximization (OSEM), maximum and posteriori

- Semimanul module form fatty acid labelling, Knauer, Germany
- **Image Quantification Software:** PMOD™, version 2.9, Pmod Technologies Ltd, Adliswil, Switzerland
- **Dose Radioisotope Calibrator:** ISOMED 2000, supplier: MED, Germany
- **Balance:** AC 211S, Sartorius AG, Germany
- **Anaesthesia system with Isoflurane Vaporiser:** Rothacher and partners, Switzerland
- **Thermometer:** TC-1000, from CWE Inc, USA
- **Common Radionuclear Device in Laboratory:** (RNL – RadioNucliren Laboratorium): Contamination monitor LB147, Berthold technologies, USA

Material for synthesis of ^{18}F-FTHA

- Duran Beakers: Sigma Aldrich, Germany
- Eppendorf vials 1,5ml: Sigma Aldrich, Germany
- Waters, Sep-PakR Accell Plus QMA Carbonate Plus Light (40 mg)
- Glass vessels with conical bottom V-Vial“)1,2 ml: Sigma Aldrich, Germany
- Glass vessels with conical bottom („V-Vial“): Grace Mini-Vial, 5,0 ml, Sigma Aldrich, Germany
- Gas bottle with Argon: Linde, Germany

5.2. Methods

5.2.1. Synthesis protocol of ^{18}F-FTHA

According to radiophisician Dr Andej Vogg form university hospital RWTH Aachen, Germany the following procedure of synthesis were applied. The step is focused on to the optimization and setting the semimanual machine for radiolabelling fatty acids and Dr. Angej Vogg provided us precious knowledge for whole procedure of radiolabelling. In the end of the synthesis protocol there is an overview of the clear orientation in synthesis process (Table 2).

1. Delivering of [^{18}F] – Fluoride isotope. Measuring of radioactivity.
2. Settings of QMA column: Accell Plus QMA Carbonate Plus Light Comlumn (40 mg) + 5 ml 1 M natriumtosylat washout, blow dry (2×5 ml air volume in syringe). QMA with 5ml HPLC-water wash out, blow dry (2×5 ml air volume in syringe). Switch on heating block to 91.6 °C. Time of heating in 3 min.
3. Preparing of Reaction vial: 5 ml V-Vial + 50 µl 0.5 M K_2C0_3 + 30 µl 1 M Kryptofix 2.2.2.
4. [^{18}F]Fluoride purification with Ar-pressure (2.0 bars) through the QMA column (Catch target – water). Wash out with: 2 ml water, 2 ml water: acetonitrile 40 : 60 Eluate with: 1 ml solution of 0,03125 M natriumtosylate, 0.375M Kryptofix 222, 40 : 60 water: acetonitrile to reaction V-vial.
5. [^{18}F]Fluoride drying V-vial (with septum and cannulas) with argon pressure 2.0 bar.

5.1.) above mentioned 1000 µl eluate, heating to 91.6 °C in heating block and dry in stream of argon.

5.2) + 1ml dry MeCN (for DNA Analysis, max. 10 ppm) cca 15 min, heating to 91.6 °C in heating block and dry in stream of argon.

5.3) + 1 ml dry MeCN (for DNA Analysis, max. 10 ppm) cca 10 min, heating to 91.6 °C in warm block and dry stream of argon.

5.4.) + 1 ml dry MeCN (for DNA Analysis, max. 10 ppm) cca 5 min, heating to 91.6 °C in warm block and dry stream of argon.

5.5) + 0.5 ml dry MeCN (for DNA Analysis, max. 10 ppm) cca 5 min, heating to 91.6 °C in warm block and dry stream of argon, leave to cool in the water bath.

5.6) visible orange residue: + 300 µl solution of precursor (0,045 M in MeCN).

6.) Labelling (above mentioned 300 µl solution of precursor),V-vial sealed system:

Heating to 91.6 °C per 15 min, let it cool in the water bat

Aliquot: 1 µl + 20 µl solution of acetonitrile and acetic acid in equal parts

+ 150 µl 0.5 M NaOH – > to solve residue

7) Saponification (row labelled solution of precursor + 150 µl 0.5 M)

Heating to 79,5 °C per 10 min, leave to cool in the water bath

-> Aliquot: 1 µl + 20 µl solution of acetonitrile and acetic acid in equal parts (finishing of the reaction)

8a) Purification: removal of [^{18}F]Fluoride (450 µl row saponification solution) + 150µl solution of acetonitrile and acetic acid in equal parts (finishing of the reaction). Go thought the SepPak Silica Plus Light column and wash out with 400 µl MeCN, than + 400 µl H_2O to filtrate 1100 µl of filtrate liquid for preparation to HPLC.
8b) Purification: removal of [^{18}F]Fluoride, HPLC-Programme ^{18}F-FTHA Computer setting: Task (with 500 µl syringe, 3x task) from HPLC to splitting preparation. Recording of production peak In V-vial: 3-6 min (1ml/min.) The final formulation: 3,3 % EtOH final

Tab. 2: The overview of the reagent which were used during the ^{18}F-FTHA synthesis

Component	Background/ use	Notice
QMA Column SepPak Carb (Waters)	Cleaning/Fixing the supplied [^{18}F]Fluorides	The activation with 5 ml 1 M NaOTs, wash out with 5ml water
1 M NaOTs	Activation of QMA	
40 : 60; H_2O : MeCN	40 : 60 water: acetonitrile	For drying of column

Component	Background/ use	Notice
QMA-eluent 1000 µl	40 : 60; 03125 M NaOTs 0,0375 M Kryptofix 2.2.2.; water: acetonitrile	
The reactor temple	50 µl 0.5 M K_2CO_3; 30 µl 1 M Kryptofix 2.2.2.	
MeCN drying by DNA-Synthesis, 100 ml in bottle	For drying the [^{18}F] Fluorides	
Solution of Precursor (SP) 300 µl	SP = 100 mg/4 ml MeCN = 45 mM	Molecule for labelling
Synthetic-HPLC column	Polymer column: PRP-1, 5 µm, 250 × 3 mm	
HPLC water	For HPLC separation	
Eluents for HPLC	85 % MeCN/ 15 % H2O + 0.5 % HOAc	
Conditions of HPLC	Isocratic, 1 ml/min, 250 bar, RT	
^{18}F-FTHA (after purification and evaporation)	+ 50 µl EtOH: +150 µl PBS + 800 µl PBS	

Component	Background/ use	Notice
Ar-gas	For dehydration	

5.2.2. Transport of ^{18}F-FTHA to Maastricht hospital

It was strictly kept the International regulation for the transport of radioactive material from place of synthesis to place of scanning. This transport was supported by German company AEREVA. The vials in volume 1 ml were transported within sealed radioprotective containers. The time of transportation from in Aachen hospital to Maastricht university hospital was approximately 30 minutes. Immediately after radiolabelling the accurate radioactivity was measured by dose calibrator in department of Nuclear Medicine in Aachen subsequently this radiopharmaceutical were measured again at the department in Maastricht. The whole synthesis was usually finished after one hour. And scanning of ^{18}F-FTHA was performed 1 hour after.

Delivering of tracer ^{18}F-FDG in volume 2 ml with activity ~500 GBq (from GE Healthcare Radiopharmaca Apotheek, Eindhoven, NL) in the morning. According to half-life of ^{18}F-FDG the radioactivity had been calibrated to certain hour 11:00 AM. It was assumed that the vial contains ~1 GBq at 8:30 AM when the scanning was usually started

.

5.2.3. Manipulation with animals

The animals were purchased from laboratory animal facility Harlan, Netherlands. Six-week old male mice were divided to two groups according to type of nutrition. The animals in the first group were fed a low fat diet (10 % kcal fat, 70 % kcal carbohydrate, 20 % kcal protein) The animals in the second group were nourished a high fat diet (45 % kcal fat, 35 % kcal carbohydrate, 20 % kcal protein). The both types of food were supplied by Research Diets, Inc., USA. Water was available ad libitum. All mice from one order

were housed with 4 cages. The maximum of animals in standard cage is 4 mice according to the Animal Experiments Committee.

For whole experiment 42 animals were ordered. One population of mice was housed two weeks until evaluation of experiment. Than the new group of mice was ordered from animal facility.

For the easily identification the every single mouse was labelled with a cut to ear which helped to identify them for multiple imaging sessions. It was necessary to record body weight and food intake for final evaluation.

The mice were housed in three different surrounding conditions. One experiment were performed under the controlled room temperature. The cages were store in animal storage room in temperature 22 °C and humidity around 46-55 %. Other surrounding condition was cold exposure. The cages were exposed to 4 °C in the fridge for 3 hours.

The third condition was warm exposure. The UV lamps we installed above to all cages. The temperature was set on 28 °C. The cages were stored in animal laboratory where a 12 h light-dark cycle (lights on from 6:30 until 18:30) were maintained. In process of scanning the mice were housed and shielded individually for the duration of the experiment to minimize inter-mouse irradiation.

5.2.4. Process of preparation for µPET scanning

All following steps are described in detail in previous thesis (Vašků, 2015) where we optimized some of these procedures of animal preparation or final evaluation of the images. The mainstay parts of this procedures will be highlighted..

Mice anaesthesia

Anaesthesia system with chamber for small animals was used. The process for complete sedating animal lasted 2-3 min in case of using 2.5-3 % isoflurane. The setting of isoflurane vaporizer machine to 2.5 % was used for induction, for maintenance 2 %, the oxygen flow was 2 L/min.

^{8}F-FTHA injections

For comfortable injecting were used syringes for application of insulin (1 ml, 100 units, 0.6 mm syringe, Therumo, Japan) When it was possible the ^{18}F-FTHA was administrated intravenously. In case of poor visible lateral tail veins the radiolabelled solution was applied to peritoneal area. The ^{18}F-FTHA was diluted with saline solution into a total volume of 200 µl per mouse for easy manipulation. . It was tried to inject dose around 10 MBq/0.2 ml per mouse. The pre- and postinjection activity of the syringe and the time of each measurement were recorded. Individual isotope doses were calibrated using radioisotope calibrator. This information was used to accurately calculate the activity administered to each individual mouse by correcting for decay

^{18}F-FDG injections

The method of application radiotracer of ^{18}F-FDG was similar like in previous ^{18}F-FTHA radiotracer (1 ml of insulin 100 units, 0.6 mm syringe). The ^{18}F-FDG was also diluted with saline solution into a total volume of 200 µl per mouse for easy manipulation. It was tried to inject the same dose as of radiotracer ^{18}F-FTHA and the pre- and postinjection activity were recorded by dose calibrator

After injection mouse was returned to individual cage for period of time 30 min. Anaesthesia was not used since image acquisition was not the objective of this work and may interfere with the radiation biology under investigation.

At the end of this part of the project, the mice were anesthetized (3 % of isoflurane) and killed by 0.4 ml of pentobarbital (200 mg/ml).

5.2.5. Standard operating procedure of PET scanning

The procedure of setting and manipulation with PET scan was described in detail in pervious diploma thesis (Vašků, 2015). The main points will be highlighted.

The tested mouse was placed to μPET horizontal automated heating bed with the controlled temperature to 37 °C.

The laser light was set up to the location of interscapular brown adipose tissue (iBAT).

The Manager software 2.4.1.1. of μPET was used to for setting, recording and data processing. The standard period of static ^{18}F-FDG imaging was 30 min of acquisition. The dynamic imaging took 20 min of scanning.

After whole scanning process, the mouse was placed back into its isolated cage while another mouse was prepared for injection.

5.2.6. Image quantification

Preclinical imagine software PMOD™ was used for our *in vivo* images evaluation. The program was installed to reserve PC with Windows XP operating system. The Formation of ROI(s) (regions of interest) were manually or semi-manually outlined. The value 20 % of threshold was experimentally determine.

5.2.7 Scanning plan of radiolabelled tracers

The plan of scanning was scheduled regarding to possibility of ^{18}F-FTHA synthesis in Aachen hospital in Germany and delivering of ^{18}F-FDG to Maastricht hospital. It had to be respected the welfare of the tested animals during the process of scanning and injection. It was required to avid the stressful and painful manipulation of mice and recuse the resulted stress to a minimum. The scanning plan were set up with respect to mice condition.

For this project the third group of mice (14 mice in each group) was used. Each group was divided to two parts. One group (two cages were fad with low fat diet and second one (other two cages) with high fat diet. During the two weeks every single mouse was scanned two times. The surrounding conditions were change when the process of scanning of whole group was done and new group of mice was ordered. First group of mice were housed in room temperature, second group in cold exposure in fridge to 4 °C and third group were housed in warm exposure 28 °C (Figure 3).

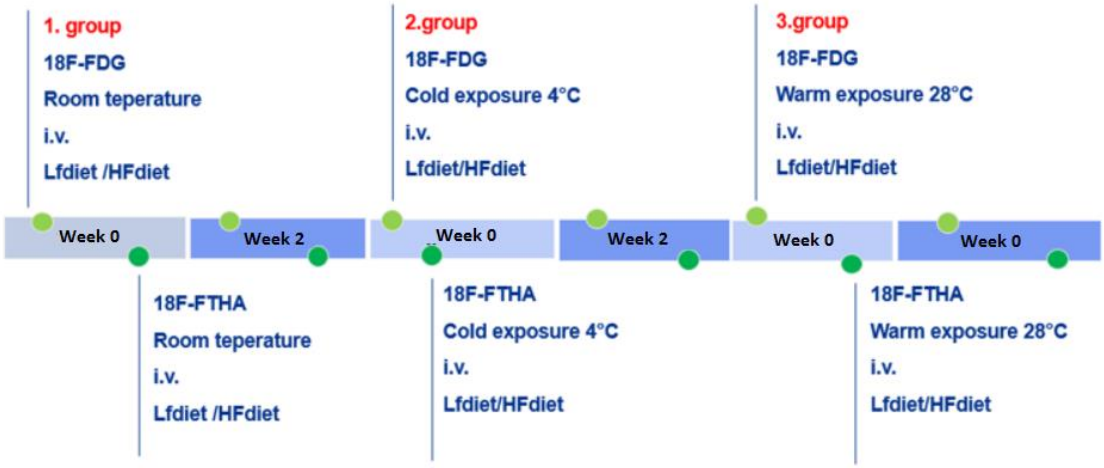

Fig. 3: Process map of PET scanning. Green dots symbolized the one day of scanning. Overall 3 groups of mice were scanned four times.

5.2.8 Statistical evaluation of final results

The data were expressed as mean +/- standard deviations. The first step of statistical comparison was to determine statistical distribution of data. Due to multiple comparison of a few parameters the One Way Anova and T-test was used.

6. Results

6.1. The yields of the ^{18}F-FTHA synthesis

The ^{18}F-FTHA product was isolated ≥ 94 % purity. Only minor radiochemical impurities (less than 6 %) were observed in the HPLC radiochromatogram (Table 3). The resulting ^{18}F-fluoro-ester was-quantitatively hydrolysed with the addition of aqueous KOH and purified by reverse-phase HPLC. Radiochemical yield of purified ^{18}F-FTHA was 45-67 %. The synthesis of ^{18}F-FTHA were performed three times and the time of one synthesis was around 50 min. The mean of injected dose was 10 MBq per mouse.

Tab. 3: The results of four synthesis performed in RWTH Uniclinic Aachen, Germany.

Sythesis	Yield (%)	Purity (%)
1.	31	67
2.	55	97
3.	52	95
4.	67	94

6.2. Weight of mice based on the intake of two different types of feeding

The weight of individual mouse was weekly recorded before the PET scanning. In day of PET scanning the maximum amount of mice was 7 per day due to time-consuming procedure. Normally, 4 mice from cage which have been fed with low fat diet and 3 mice which have been in the cage with high fat diet. The initiation weigh of mice were recorded during the week 0 and during the week 2. The data of weight intake per 2 weeks are summarized in Table 4. The overall row data are attached in Appendix 1.

Tab. 4: The records of weight gain of three group mice

1. group	No. of mice	0. week [kg]	2. week [kg]	Gain Weight [kg]
HFdiet	mouse 1	24,8	27,0	2,2
	mouse 2	21,0	21,6	0,6
	mouse 3	24,0	27,2	3,2
	mouse 4	23,1	26,4	3,3
	mouse 5	23,5	27,4	3,9
	mouse 6	22,3	23,3	1,0
	mouse 7	23,1	24,6	1,5
Lfdiet	mouse1	26,9	27,1	0,2
	mouse2	22,1	22,8	0,7
	mouse3	23,5	25,2	1,7
	mouse4	23,5	25,7	2,2
	mouse5	22,9	25,1	2,2
	mouse6	21,2	24,1	2,9
	mouse7	22,4	25,4	3,0

2. group	No. of mice	0. week [kg]	2. week [kg]	Gain Weight [kg]
HFdiet	mouse 1	27,7	28,9	1,2
	mouse 2	22,6	27,2	4,6
	mouse 3	26,5	30,0	3,5
	mouse 4	22,1	23,5	1,4
	mouse 5	26,1	26,0	-0,1
	mouse 6	24,8	27,7	2,9
	mouse 7	25,2	26,8	1,6
Lfdiet	mouse1	23,0	25,1	2,1
	mouse2	24,7	26,4	1,7
	mouse3	24,2	27,0	2,8
	mouse4	24,7	27,2	2,5
	mouse5	27,2	27,1	-0,1
	mouse6	24,0	24,4	0,4
	mouse7	24,0	25,9	1,9

3. group	No. of mice	0. week [kg]	2. week [kg]	Gain Weight [kg]
HFdiet	mouse 1	24,8	27,6	2,8
	mouse 2	22,0	24,6	2,6
	mouse 3	23,1	25,8	2,7
	mouse 4	23,0	23,8	0,8
	mouse 5	22,5	24,4	1,9
	mouse 6	20,9	22,6	1,7
	mouse 7	23,1	25,3	2,2
Lfdiet	mouse1	21,8	23,2	1,4
	mouse2	20,8	23,8	3,0
	mouse3	22,5	22,3	-0,2
	mouse4	21,8	23,8	2,0
	mouse5	21,7	23,6	1,9
	mouse6	24,2	26,1	1,9
	mouse7	21,3	22,1	0,8

The overview of overall weight gain of mice shows the Figure 4. It is evident that the mice from two group exposed to cold temperature had a highest food income then the others.

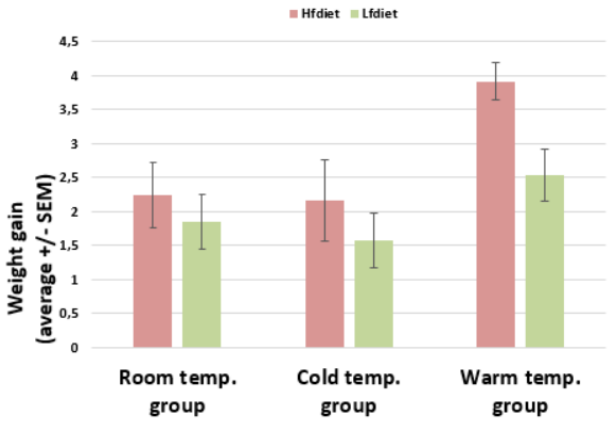

Fig. 4: The final weight gain per mouse during two weeks. The difference of weight gain related to type of feeding is statistically significant (Room tem. P = 0.044, Warm temp P = 0.042, Cold temp P = 0.031). There is no evidence to significant change between room and warm temperature but in case of cold temperature there is an enormous weight gain. (RT group vs Cold group P = 0.273, Warm group vs Cold group P = 0.262). Data are presented as means ± SEM.

During the two weeks of mice housing the food intake was recorded to determine if there is a relation related to surrounding temperature or food type. The following graph (Figure 5) shows the statistical nonsignificant differences between this conditions. According to this graph there is no changes between the temperature conditions but we can detect the difference within the group. The group which was fed with low fat diet evinced the highest food intake than group with high fat diet.

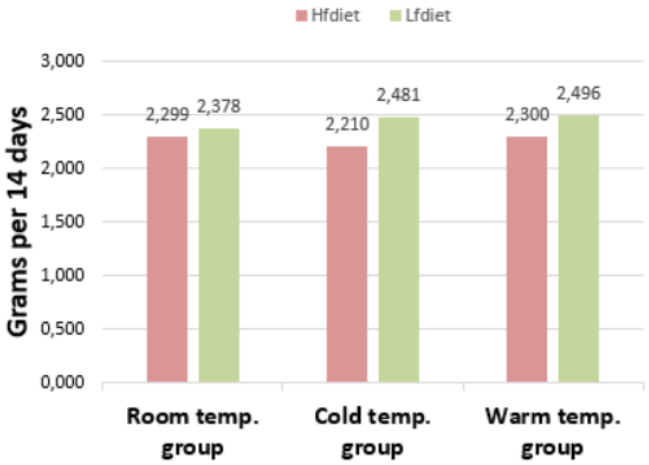

Fig. 5: Food intake per mouse during two weeks. No changes among the temperature. The P value is nonsignificant (P = 0,163). Data are presented as means.

6.3. The values of accurate adjusted doses

The injection doses of radiotracers were recorded for every single mouse. For the following calculation of SUV values was required to determine accurate adjusted dose to each mouse. The injected activity was corrected for radioactive decay between time of injection and the time of scanning. The Table 5 contains the data which were recorded during the scanning day for each mouse. The overall row data are placed in Appendix. 1.

The accurate adjusted activity was determined by weight of mouse, the amount activity of syringes before injection, time of measuring activity, injection time, activity of syringes after injection (empty syringes) and the time of measuring syringes. According to the formula (Figure 6) the actual adjusted doses were calculated.

$$At = At0 \times 2^{(-t/t1/2)}$$

Fig. 6: Formula for calculation of actual adjusted dosed. Activity at time t (At), equals activity at time zero (At0), half life time of fluoride (t1/2).

Tab. 5: The summary of data according to injected radiotracer. The units of radioactivity of tracers are MBq and the measurements were performed by radioisotope calibrator (ISOMED 2000, DE).

18F-FTHA	normal room temperature 21°C							
	Hfdiet				Lfdiet			
	cage:1				cage:4			
	mouse 4	mouse 5	mouse 6	mouse 7	mouse 4	mouse 5	mouse 6	mouse 7
	i.v.	i.v.	i.v.(p)		i.v.	i.v.(p)	i.v.(p)	i.v.->i.p.
Weight	28,4	27,6	28,1	23	26,3	26,6	25,4	24,9
s.before	15,2	8,4	9,7	Problém	6,24	7,9	8,4	6,9
time before	14:16	14:50	15:47	With	16:45	17:33	18:23	19:06
injection time	14:19	15:02	15:53	inj.	16:55	17:42	18:32	19:16
s. after	1,4	3,9	0,3		0,3	0,4	0,6	1,4
time after	14:20	15:03	15:54		16:59	17:43	18:33	19:17
Actual	14,10	5,18	9,78		6,35	7,96	8,29	5,96

The explanation of used terms: Weight – weight of mouse in day of scanning, s.before (syringe before) - radioactivity of injected dose to mouse, time before – time when the radioactivity was measured by calibrator, injection time – time when the radiotracer were injected, s. after (syringe after) – the radioactivity of empty syringe, time after – time when the empty syringe was measured, actual – the accurate injected radioactivity per mouse.

6.4. Calculation of SUV values

The SUV values were used for the final comparison. The standardized uptake value (SUV) was calculated as SUV = VOI activity multiplied *r* [kBq/ml] by mouse weight *w* [g] divided by injected dose *a'* [kBq] (Figure 7) (Dandekar et al., 2007).

$$\mathrm{SUV} = \frac{r}{(a'/w)}$$

Fig. 7: The standardized uptake value formula. Source: Dandekar et al., 2007.

The values of average voxels [kBq/cc] (cubic centimeter) were generated by PMOD software. The examples of recorded data are shown in Table 6 .and the remaining part of data from this study is listed in Appendix No. 2.

Tab. 6: The calculated values of first group of mice.

		Hfdiet								
		cage: 2			cage: 4				Average	
		mouse 1	mouse 2	mouse 3	mouse 4	mouse 5	mouse 6	mouse 7	[kBg/cc]	St. Dev
Averaged	**iBAT**	579,6393	426,5327	675,2071	625,179		596,7557	447,7812	558,5158	99,65043
[kBq/cc]	**aBAT**	317,0188	225,7732	348,4124	349,1202	436,7262	319,1782	367,0705	337,6142	63,52468
	heart	557,2033	464,756	471,2933	547,7784	501,3829	424,4324	575,1531	505,9999	55,87125
	liver	98,19212	90,46147	107,522	78,8317	95,66766	59,70896	101,4114	90,25648	16,21987
	brain	258,7696	249,3241	268,9433	228,647	277,8768	209,7532	295,8867	255,6001	29,36875
	id									
	[kBq/cc]	10880	10200	12080	10770	11460	9390	13260		
	weight	26,1	24,8	25,2	24,7	27,2	24	24		
SUV	**iBAT**	1,390495	1,037065	1,408545	1,433793		1,525254	0,810464	1,267601	0,279677
	aBAT	0,760496	0,548939	0,726821	0,800675	1,036558	0,815791	0,664381	0,764808	0,150488
	heart	1,336673	1,129995	0,983161	1,256279	1,190019	1,084811	1,041001	1,145991	0,123826
	liver	0,235553	0,219946	0,224301	0,180793	0,227065	0,152611	0,18355	0,203403	0,031062
	brain	0,620762	0,606214	0,561041	0,524381	0,659533	0,53611	0,535542	0,577653	0,051625

		Lfdiet								
		cage: 1				cage: 3			Average	
		mouse 4	mouse 5	mouse 6	mouse 7	mouse 1	mouse 2	mouse 3	[kBG/cc]	St. Dev
Averaged	**iBAT**	804,7241	495,916	429,4103		1392,608		1381,76	900,8838	465,9849
[kBq/cc]	**aBAT**	419,7966	228,7373	208,4004		543,39829		659,2777	411,922	195,9021
	heart	649,6616	370,8607	341,2279		453,62757		325,3158	428,1387	133,35
	liver	95,27389	57,87392	44,92611		124,11983		103,4364	85,12603	32,85375
	brain	247,851	198,1103	123,5447		599,45092		281,1945	290,0303	182,8695
	id									
	[kBq/cc]	10560	7490	7330	10650	10950	11710	7930		
	weight	27,7	22,6	26,5	22,1	23	24,7	24,2		
SUV	**iBAT**	2,110877	1,496355	1,552438		2,9251127		4,216721	2,460301	1,137603
	aBAT	1,101171	0,690182	0,753426		1,1413845		2,011919	1,139616	0,527619
	heart	1,704131	1,119019	1,233634		0,952825		0,992767	1,200475	0,302439
	liver	0,249914	0,174626	0,16242		0,2607083		0,315657	0,232665	0,063786
	brain	0,650139	0,597769	0,446649		1,2591207		0,858122	0,76236	0,314364

The final comparison of radiotracers is summarized in Figure 8. For statistical evaluation of differences between each group was used a parametric T-test. At first, the Normality tests were applied for determination if our data have a Gaussian distribution.

The Normality tests confirmed that our data are parametric. The Anova test were subsequently set up.

According to the final graph (Figure 8) it could be assumed that the ^{18}F-FDG has highest uptake in mice which were fed in low fat diet on the other hand there is no evidence of variability in case of type of feeding. The mice with application of ^{18}F-FDG which were housed under three different temperature had significantly higher uptake of glucose when they were fed with low fat diet than with high fat diet ($P \leq 0.005$) On the other hand the graph shows nonsignificant difference between types of feeding in case of radiotracer ^{18}F-FTHA ($P = 0.881$). After two weeks the influence of low fat nutrition wasn't high the amount of ^{18}F-FDG uptake was slightly decreased. If we compare the influence of surrounding temperature we can detect that the highest uptake was in mice which have been exposed to cold temperature.

The detailed comparison is summarized in Appendix No. 4. We used Anova comparison for each parameters (overall 276 statistical comparison).

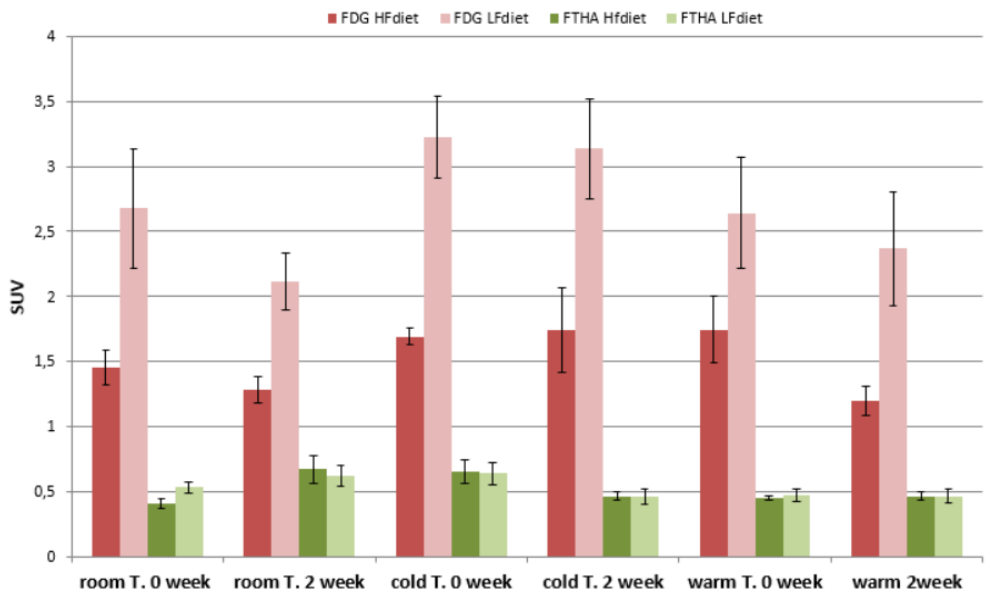

Fig. 8: Comparison of surrounding conditions to the intensity of uptake in iBAT. Data are presented as means ± SEM.

6.5. The final comparison volume of iBAT

In first part of this project was evaluated the suitable percentage of threshold volumes. Based on this gained knowledge the 20 % reduction of threshold was applied. We used this setting for each threshold for maintaining the constant volumes to final comparison. According to the Figure 9 and Table 6, we can suppose that the ^{18}F-FDG has higher influence to iBAT volume than ^{18}F-FTHA. The statistical analysis confirm this hypothesis. The overall difference is P = 0.0009 (evaluation by GraphPad Prism software).

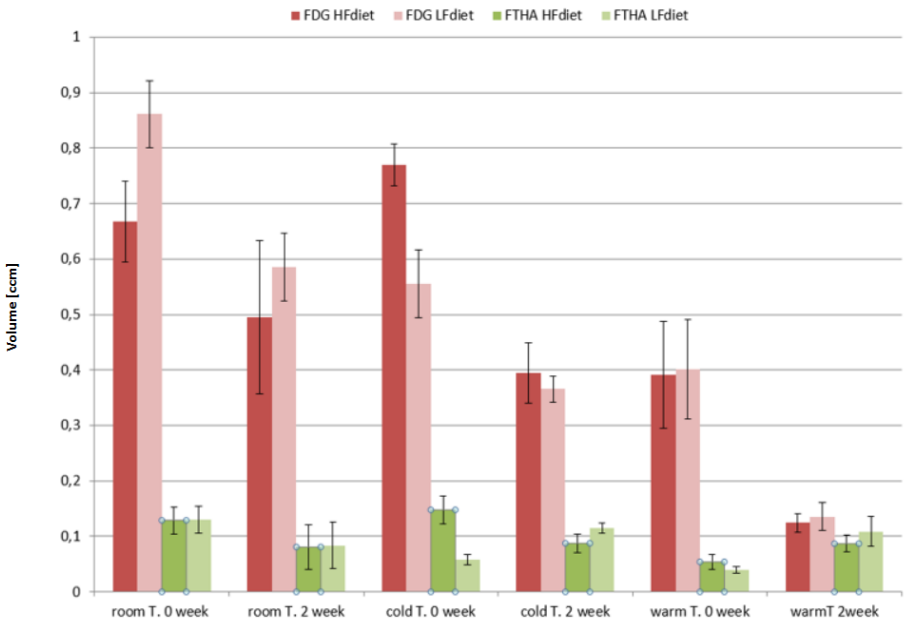

Fig. 9: Comparison of iBAT volume in different surrounding conditions and radiotracers. Data are presented as means ± SEM. [ccm] – cubic centimeter

Tab. 7: The summarized data of average volume in iBAT regions

			room T. 0 week	room T. 2 week	cold T. 0 week	cold T. 2 week	warm T. 0 week	warm T. 2 week
Average volume [ccm]	FDG	HF	0,668	0,496	0,770	0,395	0,391	0,124
		LF	0,861	0,585	0,556	0,366	0,401	0,135
	FTHA	HF	0,129	0,081	0,148	0,088	0,054	0,087
		LF	0,130	0,083	0,058	0,115	0,040	0,109
ST.DEV.	FDG	HF	0,265	0,157	0,102	0,140	0,254	0,045
		LF	0,015	0,301	0,161	0,060	0,238	0,066
	FTHA	HF	0,047	0,080	0,052	0,030	0,027	0,029
		LF	0,124	0,020	0,012	0,010	0,011	0,052

6.6. Visualization of iBAT by PMOD™ software

6.6.1. Interscapular iBAT in different angels

The ^{18}F-FDG μPET scan allowed the quantification and visualization of glucose and fatty acids metabolism throughout the whole body of mice. These following images show the single location of iBAT and other organs depending on radiotracers, surrounding condition and feeding. For these final images we used the corrections in PMOD™ software which were set up and validated in previous thesis (Vašků, 2015).

The Figure 10 shows the largest and the best recognizable brown fat is interscapular depot in various angles. The position of iBAT is between scapulas above the spine. However, the following images can be inaccurate. In case of high uptake of radiotracer especially ^{18}F-FDG the signals are spread to surroundings. According to the Figure 10 (C) the iBAT appears like shape of butterfly which is common name from sagittal section.

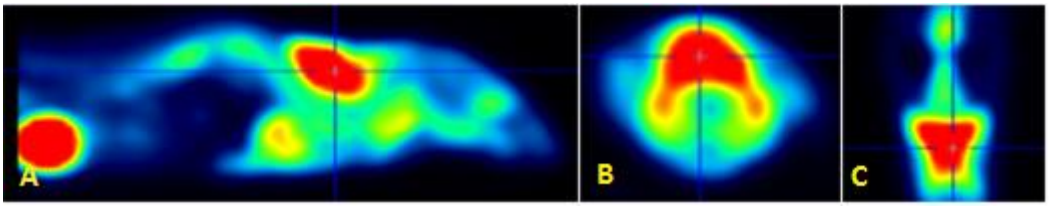

Fig. 10: μPET imaging of iBAT in three planes of section: (a) axial, (b) coronal, (c) sagittal.

6.6.2. Distribution of uptake ^{18}F-FDG in mice

The ^{18}F-FDG radiotracer is suitable chemical how visualise iBAT in good quality. The process of glucose trapping by metabolic active tissues are excellent visible in Figure 11. After specific postinjection time (30 min) the most activity accumulation was in the urinary bladder.

In the abdominal cavity the liver showed an inconsiderable uptake of ^{18}F-FDG. It is demonstrated like black spot in the middle of abdomen. The other structures of tissues (muscle, white fat) were not detected. The skeletal muscle's uptake was low or none at rest.

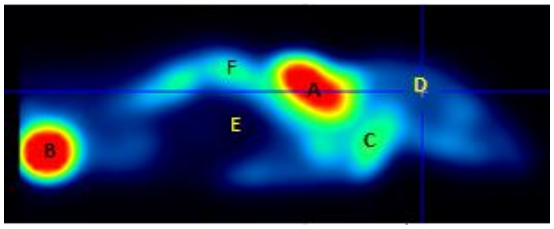

Fig. 11: The localization of active glucose consumption in mice. A) iBAT, B) bladder, C) heart, D) brain, E) liver, F) diaphragma muscle/auxilliary BAT.

6.6.3. Distribution of uptake ^{18}F- FTHA in mice

The *in vivo* major distribution and metabolism of ^{18}F-FTHA are in heart and liver as we expected. There is obvious that the brain do not use fatty acid lake first fuel for metabolic function and it appears like dark spots (Figure 12).

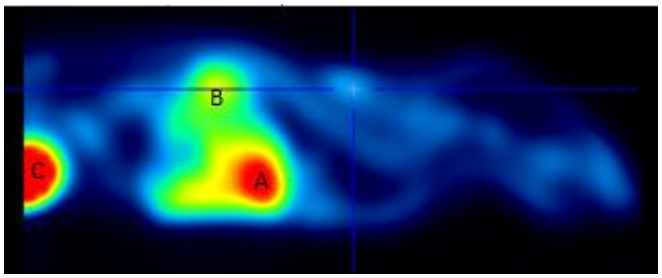

Fig. 12: The example of ^{18}F-FTHA uptake in different regions. A) heart, B) liver C) bladder

6.6.4. PET imaging of dead mouse

This image was performed with euthanized mouse. After 5 min of intravenous injection of ^{18}F-FDG the mouse was anesthetized and euthanatized by 0.4 ml pentobarbital (200 mg/ml, Abbott, USA). The image (Figure 13) shows the high uptake in brain and surroundings in comparison with *in vivo* distribution of ^{18}F-FDG. We can assumed that the euthanasia has an influence of the trapping glucose in mouse brain.

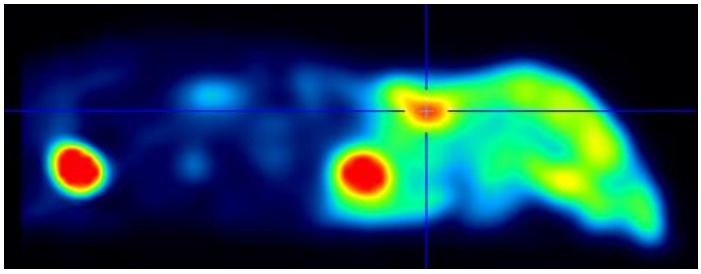

Fig. 13: The scan of dead mouse. It shows the height uptake in brain which is the main difference between scan of in vivo distribution of **^{18}F**-FDG.

6.7. Final comparison of radiotracers

6.7.1. The visualization of ^{18}F-FDG radiotracer in different surrounding condition and feeding

According to following images Figure 14; 15, 16 we can suppose that uptake of ^{18}F-FDG in iBAT correlates with type of feeding and it is related to surrounding temperature as well. The trapping of glucose is higher in mice which were fed with LF diet than in mice fed with nutrition rich food. The biggest spot of iBAT is localized in mouse which were exposed to cold temperature. On the other hand the lowest glucose uptake we detected in mouse witch were fed with HF diet in warm exposure. In this image the iBAT shows the minor metabolic activity.

- **Room temperature (21 °C)**

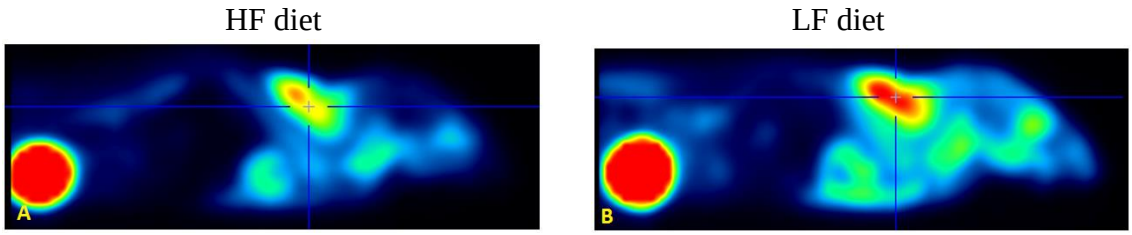

Fig. 14: Two scans of mice which were housed in room temperature. Image A shows lower uptake in iBAT than mice on the image B.

- **Cold temperature (4 °C)**

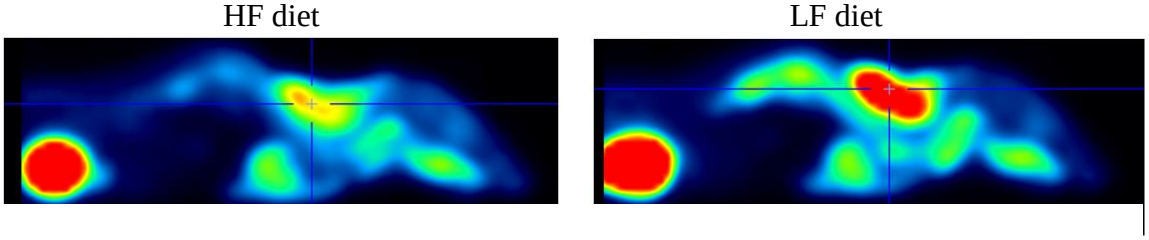

Fig. 15: Images of two mice which were exposed to cold temperature. Mouse was fed with low fat diet had a higher uptake of ^{18}F-FDG than mouse was fed high feet diet**.**

- **Warm temperature (28 °C)**

HF diet LF diet

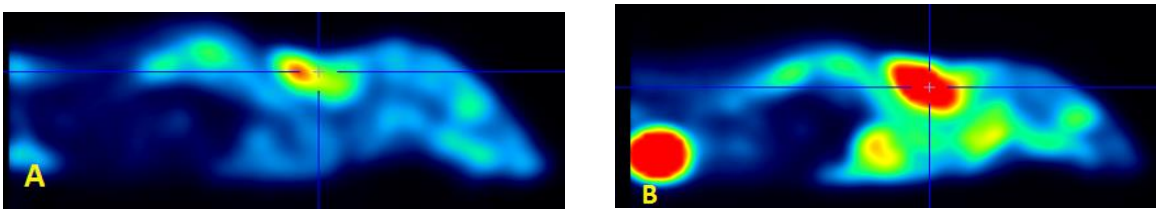

Fig. 16: The images show the difference between uptake of ^{18}F-FDG. The image A shows the lower activity than image B

6.7.2. The visualization of ^{18}F-FDG radiotracer in different surrounding condition and feeding

The ^{18}F-FTHA uptake seems to be nutrition nondependent radiotracer. There is no evidence that type of feeding plays main role for the trapping of fatty acids. It is obvious that the highest concentration of radiotracer ^{18}F-FTHA is in the liver, heart and bladder (Figure 17; 18; 19). The explanation of hypothesis corresponded with SUV form PMOD™ software.

- **Room temperature (21 °C)**

HF diet LF diet

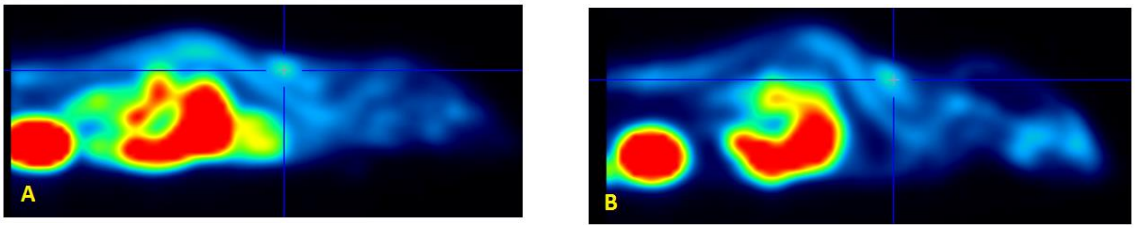

Fig. 17: According to these images of ^{18}F-FTHA there is no difference between types of feeding. The brown spots are poor visible.

- **Cold temperature (4 °C)**

HF diet LF diet

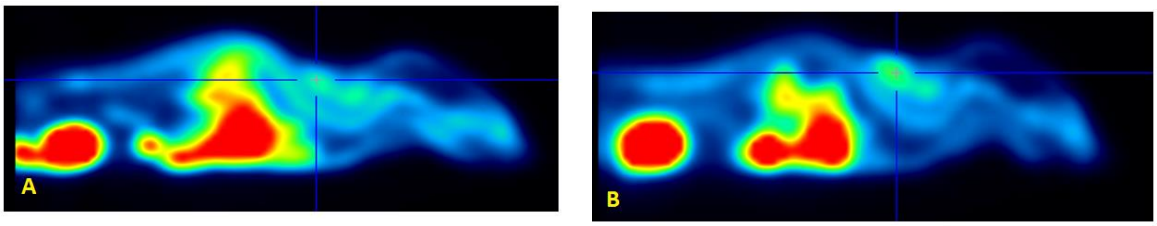

Fig. 18: The images show the main radioactivity in heart and liver but the brow adipose spots are poor visible in both cases of feeding.

- **Warm temperature (28 °C)**

HF diet LF diet

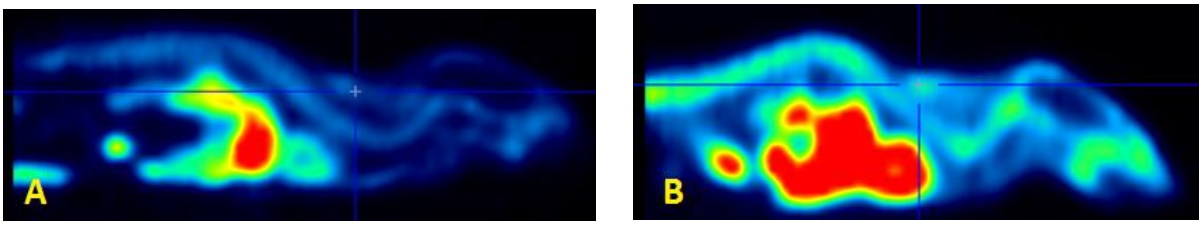

Fig. 19: Mice which were housed under 28 °C did not have higher uptake in brow adipose areas in comparison with other surrounding condition**.**

7. Discussion

The whole project was supported by the department of Nuclear Medicine in Maastricht, Netherlands and was performed under the tutelage Dr Matthias Bauwens. Among his projects belong the investigation of function interscapular brown adipose tissue (iBAT) via noninvasive methods such as μPET, μSPECT, μCT and others. This project was divided to two parts. First aims of study were set up and optimization of the process of brow adipose tissue scanning for the purpose to get a visible and easy quantified the interscapular brown spots. In this initial study, we have achieved the practical skills, which involves the handling of animals and correct process of injection of radiotracers. Second part of project was to determine what kind of positron emission tomography (PET) radiotracer is more suitable for interscapular imaging of brown adipose tissue and these results should help us to understand glucose and fatty acid metabolism of iBAT. Due to cooperation with RWTH Uniclinic Aachen in Germany, we were able to radiolabell fatty acid by isotope ^{18}F. The synthesis was performed in semimanual machine for fatty acid labelling. Dr. Andreas Vogg from department of Nuclear Medicine in RWTH Uniclinic Aachen was helpful during the setting of radiolabeling machine. He gave us a valuable advice and support in process of synthesis.

The ^{18}F-FTHA tracer is commonly used to study fatty acid metabolism in human heart and skeletal muscle. This tracer is trapped by high energy consumption tissues which iBAT demonstrates. The ^{18}F-FTHA synthesis was performed four times but first synthesis had a low yield and high impurities in product (31 % yield). This bad result was caused by incorrect setting of synthesis software. This product of ^{18}F-FTHA was excluded from the evaluation and final comparison. The values of actual injected dose of ^{18}F-FTHA were broad range. This values were variable due to way of intravenous administration of radiotracers. It depends on the methods of manipulation with animals and dexterity how to correctly applicate the radiotracers. In case of impossibility if application radiotracers we injected the dose intraperitoneally in purpose to visualise at least small depot of iBAT. In some of cases the injection of radiotracer ^{18}F-FTHA were missed due to poor visibility

of tail vein. It was tried two times but radiotracer were spitted to the surrounding tissue. The tested mouse was excluded from scanning that day.

Radiotracer ^{18}F-FDG was described in details in diploma thesis (Vašků, 2015). We detected the high quality visualisation of iBAT in mice in each surrounding condition and type of feeding. Nevertheless, the images from the PET scan showed high uptake of ^{18}F-FDG in bladder and other parts of the body. This is in accordance with the finding that ^{18}F-FDG is excreted by the kidneys without resorption in the renal proximal tubules and is continuously accumulated in the bladder (Wong et al., 2013). Among the other highly energetic dependent tissue is myocardium, but this spot showed the low intensity of glucose uptake than iBAT. It is necessary to mention, that anaesthesia has an influence on ^{18}F-FDG uptake in mouse brain (Hiroshi, 2003) that can explain why the images showed the poorly visible brain and on the other hand the isoflurane significantly increases the heart uptake. The two visible spots of along the spine remain unclear. In previous diploma thesis we used gamma counter for the determination and understanding if these spots are auxiliary BAT of part of active diaphragm muscle. Diaphragm muscle also consumes glucose due to active respiration. The two available studies have an opposed explanation. After measurement of activity via gamma counter we suppose that it would be a mixture of these two areas (Vašků, 2015).

Although we tried to keep the setting during the whole process of comparison same there are the few discrepancies. Such as the ^{18}F-FDG has higher iBAT volume in case of high fat diet than low fat diet under cold temperature. The SUV measuring are much more accurate and give us more information about uptake of radiotracer than the observation to volumes. One of the reason of this inaccuracy is human factor. The important feature is the acquisition of certain skills when evaluating the slide in PMOD™ software. It depends directly on the personal ability to create a large border around the object of interest when setting colour scroll bar. The same images, which are evaluated by different people, may differ due to subjective point of view.

During the project we monitored the parameters related to mouse feeding such as the weight gain and food intake per mouse. We detected that the mouse exposed to warm

temperature had the highest weight gain than mouse exposed to cold or room temperature. This hypothesis correspond with the study of researcher Moellering DR (2012). He claims that the ambient temperature is a significant contributor to energy intake and energy expenditure. However the food intake was in each case almost the same. For this result is easy explanation which is related to the mouse movement during the day. We observed that the mice in warm condition had not to movement in cage like mice in room or cold temperature.

IBAT is activated by the catecholamine released from sympathetic nerve endings via β_3-adrenergic receptors. This stimulation leads to high-level expression of uncoupling protein-1 (UCP1) on the inner membrane of mitochondria, which can burn glucose and fatty acids to produce heat through a process known as non-shivering thermogenesis. On the contrary, the warmer housing or surgically denervated BAT shows reduction of expression UCP1 and other thermogenic factors (Harms et al., 2013) Generally, we can assume that the type of feeding has an influence to ^{18}F-FDG trapping by iBAT. There is a statistical significance between low fed diet and high fat diet. Mice fed with low fat diet showed the higher uptake of ^{18}F-FDG. We supposed that the higher percentage of carbohydrates in high fat diet caused the insensitivity of iBAT to trapping ^{18}F-FDG radiotracer. On the other hand we did not detected significant difference between types of feeding in case of ^{18}F-FTHA.

One of the iBAT function is the clearance of triglycerides from the circulation. BAT has triglyceride stores deposit in small lipid droplets and fatty acids are rapidly delivered from these droplets for fuel in activated mitochondria (De Meis et al, 2012). We expected the high uptake of long chain fatty acid radiotracer but we detected only minor spots in comparison to ^{18}F-FDG. Our hypothesis of poor vision of iBAT of low SUV value is that myocardium as high energy consumption muscle had trapped the major part of the ^{18}F-FTHA. It is know that the myocardial muscle has a high fatty acid uptake due to high rate of β-oxidation. Hepatic clearance of radioactivity showed excellent visible images of liver (Figure 17-19).

The next steps of this project will lead to investigate lipid storage and using the Hounsfield units (HU), which are derived from Computer Tomography (CT) images based on tissue densities (water content). This capacity may be used for the determination of active vs. nonactive BAT, such as in cold and in warm (Hu and Gilsanz, 2011). Another option for the noninvasive estimation of BAT lipid storage is Magnetic Resonance Imaging (MRI). This method is based on the spin effect of water molecules thus the tissue content of water may be used for the tissue differentiation. This are others aims which would be investigated in the future.

8. Conclusion

1. We radiolabelled fatty acid by isotope ^{18}F in sufficient yield ($\geq$ 55 %) and purity ($\geq$ 94 %) for the purpose of visualisation of brow adipose tissue through a μPET scan. This radiotracer was transported from Aachen hospital in Germany to Maastricht hospital, Netherlands in adequate radioactivity which was necessary for imaging brown fat in mice.

2. We compared SUV values two radiotracers ^{18}F-FTHA and ^{18}F-FDG in different surrounding conditions such as room (21 °C), cold (4 °C) and warm (28 °C) temperature and also depending on type of nutrition low fat diet and high fat diet. According to these results we are able to claim that the radiotracer ^{18}F-FDG has a significantly highest uptake in metabolic active brown fat (SUV = 3.22 kBq/cc) in case of low fat diet and cold temperature. In comparison with ^{18}F-FTHA when the surrounding condition and type of feeding did not change the fatty acid trapping (SUV = 0.46 kBq/cc). The radiotracer ^{18}F-FDG has a better resolution, image quality and higher uptake by iBAT than radiotracer ^{18}F-FTHA.

9. References

Cypess AM, Lehman S, Williams G, Tal, Rodman D, Goldfine AB, Kuo FC, Palmer EL et al. Identification and Importance of Brown Adipose Tissue in Adult Humans. The New England Journal Medicine 2009; 360(15): 1509–1517.

Anderson CM, Kazantzis M, Wang J, Venkatraman S, Goncalves RL, Quinlan CL, Ng R, Jastroch M et al. Dependence of Brown Adipose Tissue Function on CD36-Mediated Coenzyme Q Uptake. Cell Press 2015; 10(4): 505–515.

Baum S. Radiochemische Untersuchungen der kritischen Reaktionsparameter bei der Darstellung der Fettsäure 14-(R,S)-[18F]Fluor-6-thia-heptadecansäure. Bechelor work, 2013. RETH Aachen University. Department of Nuclear Medicine.

Beaven WS, Tontine P. Nuclear Receptors in Lipid Metabolism: Targeting the Heart of Dyslipidemia. Annual Review of Medicine 2006; 57: 313-329.

Berge RK, Skorve J, Tronstad KJ, Berge K, Gudbrandsen OA, Grav H. Metabolic effects of thia fatty acids. Current Opinion in Lipidology 2002; 13(3): 295-304.

Bergmann SR, Herrero P, Sciacca R, Hartman JJ, Rubin PJ, Hickey KT, Epstein S, Kelly DP. Characterization of altered myocardial fatty acid metabolism in patients with inherited cardiomyopathy. Journal of Inherited Metabolic Disease 2001; 24(6): 657-674.

Bonen A, Campbell SE, Benton CR, Chabowski A, Coort SL, Han XX, Koonen DP, Glatz et al. Regulation of fatty acid transport by fatty acid translocase/CD36. The Proceedings of the Nutrition Society. 2004; 63(2): 245-249.

Chaves VE, Frasson D, Martins-Santos MES, Migliorini RH. Fatty acid synthesis and generation of glycerol-3-phosphate in brown adipose tissue from rats fed a cafeteria diet. Canadian Journal Physiology and Pharmacology. 2008; 86(7): 416-423.

Tews D, Wabitsch M. Renaissance of Brown Adipose Tissue Hormone Research in Paediatrics 2011; 75: 231–239.

Degrado T, Coenen HH, Stocklin G. Synthesis of 14 (R,S)-[18F]fluoro-6-thia-heptadecanoic acid (FTHA). Journal of Labelled Compounds 1989; 30(7): 1211–1218.

De Meis L, Ketzer LA, Camacho-Pereira J, Galina A. Brown adipose tissue mitochondria: modulation by GDP and fatty acids depends on the respiratory substrates. Bioscience Report 2012; 32(1): 53-59.

Eberlé D, Hegarty B, Bossard P, Ferré P, Foufelle F. SREBP transcription factors: master regulators of lipid homeostasis. Biochimie 2004; 86(11): 839-848.

Fillmore N, Abo Alrob O, Lapaschuk GD. Fatty Acid beta-Oxidation. AOCS lipid library 2011; 24(2): 325-328.

Geltman EM. Assessment of myocardial fatty acid metabolism with 1-11C-palmitate. Journal of Nuclear Cardiology 1994; 1(2): 15-22.

Hagberg CE, Falkevall A, Wang X, Larsson E, Huusko J, Nilsson I, van Meeteren LA, Samen E at al. Vascular endothelial growth factor B controls endothelial fatty acid uptake. Nature 2010; 464: 917-921.

Halvorson I, Gregor L, Thornhill JA. Brown adipose tissue thermogenesis is activated by electrical and chemical (L-glutamate) stimulation of the ventromedial hypothalamic nucleus in cold-acclimated rats. Brain Research 1990; 522(1): 76-82.

Lao Y, Yang C, Zou W, Gan M, Chen P, Su W. Quantification of Kryptofix 2.2.2 in [18F]fluorine-labelled radiopharmaceuticals by rapid-resolution liquid chromatography. Nuclear medicine communication 2012; 33(5): 498-502.

Marchington JM, Pond CM. Site-specific properties of pericardial and epicardial adipose tissue: the effects of insulin and high-fat feeding on lipogenesis and the incorporation of fatty acids in vitro. International Journal of Obesity 1990; 14(12): 1013-1022.

Moerlein SM, Brodack JW, Siegel BA, Weich MJ. Elimination of contaminant Kryptofix 2.2.2 in the routine production of 2-[18F]fluoro-2-deoxy-D-glucose. International Journal of Radiation and Applications and Instrumentation Part A 1989; 40(9): 741-743.

Pandey MK, Bansal A, DeGrado TR. Fluorine-18 labelled thia fatty acids for PET imaging of fatty acid oxidation in heart and cancer. Heart Metabolism 2011; 51: 15–19.

Peterson LR. Clinical Implications of Molecular Imaging Research. Radionuclide Imaging of Myocardial Metabolism 2010; 3: 211-222.

Renstorm B, Renstrom B, Rommelfanger S, Stone CK, DeGrado TR, Carlson KJ, Scarbrough E, Nickles RJ et al. Comparison of fatty acid tracers FTHA and BMIPP during myocardial ischemia and hypoxia. Journal of Nuclear Medicine 1998; 39(10): 1684-1689.

Runkle AC, Shao X, Tluczek LJ, Henderson BD, Hockley BG, Scott PJ. Automated production of [11C]acetate and [11C]palmitate using a modified GE Tracerlab FX(C-Pro). Applied Radiation and Isotopes 2011; 69(4): 691-698.

Takeyama D, Kagaya Y, Yamane Y. Effects of chronic right ventricular pressure overload on myocardial glucose and free fatty acid metabolism in the conscious rat. Cardiovascular Research 1995; 29(6): 763-767.

Vašků T. Molecular imaging of brown adipose tissue in mice. Diploma thesis, 2015. Charles University in Prague. Faculty of Pharmacy in Hradec Králové.

Wu Q, Kazantzis M, Doege H, Ortegon AM, Tsang B, Falcon A, Stahl A. Fatty acid transport protein 1 is required for nonshivering thermogenesis in brown adipose tissue. Diabetes. 2006; 55(12): 3229-32237.

Wu Z, Satterfield MC, Bazer FW, Wu G. Satterfield MC, Bazer FW, Wu G. Regulation of brown adipose tissue development and white fat reduction by L-arginine. Current Opinion in Clinical Nutrition and Metabolic Care 2012; 15(6): 529-538.

Yinlin L, Huang T, Zhang X, Zhong M, Walker NN, He J, Berr SS, Keller SR et al. Determination of Fatty Acid Metabolism with Dynamic 11C-Palmitate Positron Emission Tomography of Mouse Heart In Vivo. Molecular Imaging 2015; 14: 516–525.

Zhude Tu, Shihong L, Sharp TL, Herrero P, Dence CS, Gropler RJ, Mach RH. Synthesis and Evaluation of 15-(4-(2[18F]Fluoroethoxy)phenyl) pentadecanoid Acid: a Potential PET Tracer for Studying Myocardial Fatty Acid Metabolism. Bioconjugate Chemistry 2010; 21(12): 2313–2319.

8.1. Book sources

Berg JM, Tymoczko JL, Stryer. Fatty Acid Metabolism. Biochemistry. New York: W H Freeman. 2002: 56-70. ISBN 071673051.

Bernlohr DA, Banaszak L. Lipid binding proteins within molecular and cellular biochemistry. Dordrecht; Boston, Mass, Kluwer Academic. 1999: 34-41. ISBN 0792382234.

Shu-xin Z. An atlas of histology. New York: Springer. 1999:316-386. ISBN 0387949542.

Vasken D, Gerald MP. Cardiac CT, PET and MR. New Jersey: John Wiley & Sons. 2008:164-171. ISBN 1405171715.

Appendix No. 1:

The records of row data from scanning days. These following parameters are recorded. Weight – weight of mouse in day of scanning, s. before (syringe before) - radioactivity of injected dose to mouse, time before – time when the radioactivity was measured by calibrator, injection time – time when the radiotracer were injected, s. after (syringe after) – the radioactivity of empty syringe, time after – time when the empty syringe was measured, actual – the accurate injected radioactivity per mouse.

18F-FDG	normal room temperature					
	Hfdiet			Lfdiet		
	cage:2			cage:3		
	mouse 1	mouse 2	mouse 3	mouse 1	mouse 2	mouse 3
administration	i.p.	i.p.	i.p.	i.p.	i.p.	i.p.
Weight	26	27,7	26,8	25,1	26,4	27
s.before	13,7	11,60	9	9,58	9,8	6,9
time before	12:13	12:49	13:34	14:01	14:44	15:19
injection time	12:15	12:50	13:35	14:02	14:45	15:25
s. after	0,3	0,50	0,2	0,1	0,2	0,1
time after	12:16	15:50	13:35	14:02	14:46	15:26
Actual	13,58	11,51	8,86	9,54	9,66	7,07

18F-FDG	normal room temperature							
	Hfdiet				Lfdiet			
	cage:1				cage:4			
	mouse 4	mouse 5	mouse 6	mouse 7	mouse 4	mouse 5	mouse 6	mouse 7
administration	i.v.	i.v.	i.v.	i.v.	i.v.	i.v.	i.v.	i.v.
Weight	28,9	27,2	30	23,5	27,2	27,1	24,4	25,9
s.before	13	11,4	11,4	10,5	6,6	5,2	7,7	5,6
time before	9:46	10:20	10:56	11:39	13:37	14:13	14:45	15:42
injection time	9:51	10:25	11:04	11:44	13:40	14:15	14:56	15:45
s. after	0,5	0,7	0,7	0,7	0,2	0,1	1,8	0,7
time after	9:52	10:26	11:05	11:44	13:41	14:17	14:59	15:46
Actual	12,92	11,07	11,29	10,14	6,53	5,17	6,49	5,01

18F-FTHA	normal room temperature							
	Hfdiet				Lfdiet			
	cage:1				cage:4			
	mouse 4	mouse 5	mouse 6	mouse7	mouse 4	mouse 5	mouse 6	mouse 7
administration	i.v.(p)	i.v./i.p	i.v.	i.vp	i.vp	i.v.(p)	i.v.	i.v./i.p
weight	28,7	26,3	29,6	27,6	26,2	26,7	24,4	25,4
s.before	4,3	6,6	10,6	7,28	8,9	5,8	3,63	7,51
time before	14:16	15:38	14:50	19:19	16:27	17:12:00	17:53	18:35
injection time	14:19	15:43	14:54	19:23	16:33	17:15	18:00	18:38
s. after	0,2	2,74	1,85	1,87	3,51	2,6	1	2,55
time after	14:21	15:47	14:55	19:24	16:34	17:17	18:01	18:39
actual	4,18	4,14	9,03	5,61	5,75	3,34	2,80	5,12

18F-FDG	cold exposure 4C							
	Hfdiet				Lfdiet			
	cage:1				cage:4			
	mouse 1	mouse 2	mouse 3	mouse 4	mouse 4	mouse 5	mouse 6	mouse 7
administration	i.v.	i.v.	i.v.	i.v.	i.v.	i.v.	i.v.	i.v.
weight	24,8	22	23,1	23	21,8	8,64	24,2	21,3
s.before	12,6	11,35	8,45	11,45	7,8	8,64	6,5	7,35
time before	9:46	10:22	11:03	11:38	13:01	12:15	13:38	14:23
injection time	9:49	10:25	11:05	11:42	13:03	12:21	13:42	14:25:00
s. after	0,45	1,78	0,334	3,93	1,38	0,07	1,7	0,51
time after	9:43	10:27	11:06	11:44	13:04	12:23	13:44	14:27
actual	12,37	9,81	8,23	7,86	6,53	8,90	4,99	6,94

18F-FTHA	cold exposure 4°C					
	Hfdiet			Lfdiet		
	cage: 2			cage: 3		
	mouse 5	mouse 6	mouse 7	mouse 1	mouse 2	mouse 3
administration	i.v.	i.v.	i.v.	i.v.	i.v.	i.v.
weight	22,5	20,9	23,1	21,8	20,8	22,5
s.before	40,4	22,8	21,9	17,3	12,35	9,35
time before	14:40	15:12	15:55	16:30	17:05	17:47
injection time	14:42	15:14	15:57	16:34	17:10	17:49
s. after	18:01	6,57	5,9	12,2	2,42	0,9
time after	14:43	15:15	15:38	16:36	17:11	17:50
actual	40,17	16,56	15,53	5,69	10,34	8,57

18F-FTHA	cold exposure 4C							
	Hfdiet				Lfdiet			
	cage: 1				cage: 4			
	mouse 1	mouse 2	mouse 3	mouse 4	mouse 4	mouse 5	mouse 6	mouse 7
administration	i.v.	i.v.	i.v.	i.v.	i.v.	i.v/i.p.	i.v.	i.v.
weight	25,4	23,5	22,3	22,3	22,3	22,8	24	21,1
s.before	11,4	10,3	6,47	7,1	35,6	12,8	20,1	14,8
time before	17:26	18:13	18:47	19:30	14:52	15:29	16:05	16:51
injection time	17:31	18:14	18:54	19:33	14:55	15:30	16:13	16:52
s. after	2,21	5,03	5,03	0,9	16,2	3,3	9,5	4,9
time after	17:32	18:14	18:55	19:34	14:56	15:31	16:14	16:53
actual	9,57	5,34	1,76	6,34	20,18	9,60	11,70	10,02

18F-FDG	cold exposure 4°C							
	Hfdiet				Lfdiet			
	cage:1				cage:4			
	mouse 1	mouse 2	mouse 3	mouse 4	mouse 4	mouse 5	mouse 6	mouse 7
administration	i.vp	i.vp	i.vp	i.vp	i.vp	i.vp	i.vp	i.vp
weight	27,6	25,3	25,6	23,8	24,2	25	26,1	22,1
s.before	11,52	13,81	14	9:36	9,57	10,7	10,38	8,6
time before	9:39	10:17	11:40	10:59	12:22	13:07	13:46	14:30
injection time	9:44	10:19	11:44	11:00	12:26	13:09	13:48	14:31
s. after	1,16	0,35	8,1	8:18	4,07	1,357	3,39	0,529
time after	9:45	10:19	11:45	11:01	12:27	13:10	13:51	14:32
actual	10,01	13,29	5,60	10,98	5,29	9,22	6,92	8,02

18F-FDG		warm exposure 4°C					
	Hfdiet			Lfdiet			
	cage:1			cage:3			
	mouse 1	mouse 2	mouse 3	mouse 1	mouse 2	mouse 3	mouse 4
administration	i.p.	i.p.	i.p.	i.p.	i.v.+i.p.	i.p.	i.p.
weight	23,2	23,8	24,9	24,5	23,1	21,5	22,1
s.before	10,3	9,1	12,63	6,7	7,36	6,88	8,6
time before	9:40	10:25	11:08	11:47	12:29	13:18	14:04
injection time	9:41	10:27	11:11	11:49	12:36	13:21	14:04
s. after	0,9	3,21	2,68	0,4	1,4	0,9	2,54
time after	9:43	10:28	11:12	11:50	12:40	13:30	14:04
actual	9,35	5,80	9,73	6,22	5,68	5,90	6,06

18F-FDG	warm exposure 28°C						
	Hfdiet				Lfdiet		
	cage:2				cage:4		
	mouse 4	mouse 5	mouse 6	mouse 7	mouse 5	mouse 6	mouse 7
administration	i.p.	i.p.	i.p.	i.p.	i.p.	i.p.	i.p.
weight	26,1	24,1	24,7	21,5	24,6	23,7	21,3
s.before	17,3	14,1	11,5	9,7	20,3	24,1	18,3
time before	13:26	13:54	14:39	15:13	8:58	9:28	10:06
injection time	13:27	13:59	14:40	15:19	9:00	9:28	10:09
s. after	2,03	1,3	1,2	1,3	1,7	1,7	1,6
time after	13:27	14:00	14:40	15:19	9:01	9:29	10:10
actual	15,16	12,37	10,23	8,04	18,36	22,41	16,37

18F-FTHA	warm exposure 28°C							
	Hfdiet			Hfdiet	Lfdiet			Lfdiet
	cage: 1			cage: 2	cage:4			cage: 3
	mouse 4	mouse 5	mouse 6	mouse 7	mouse 1	mouse 2	mouse 3	mouse 4
administration	i.vp.	i.vp.	i.vp.	i.vp + ip	i.vp.	i.vp.	i.vp.	i.vp
weight	25	27,2	27,3	24,5		22	25,5	25,2
s.before	25	10,10	10	30,3		12,5	11,5	13,4
time before	13:50	14:25	15:13	15:17		16:38	17:26	18:02
injection time	13:55	14:30	15:14	15:19		16:45	17:28	18:05
s. after	1,1	0,50	0,8	1,9		0,9	2,20	1
time after	14:20	14:29	15:15	15:20		16:46	17:32	18:08
actual	23,28	9,28	9,14	28,03	0,00	11,07	9,21	12,17

18F-FTHA	warm exposure 28°C							
				Hfdiet	Lfdiet			Lfdiet
	cage: 1			cage: 2	cage:4			cage: 3
	mouse 1	mouse 2	mouse 3	mouse 4	mouse 5	mouse 6	mouse 7	mouse 1
administration	i.vp.	i.vp.	i.vp.	i.vp	i.vp.	i.vp.	i.vp.	i.vp
weight	23,4	23,4	25,1	26,2	24,7	23,6	21,8	25,3
s.before	20,1	11,70	12,6	6,18	9,2	7,75	7,1	6,32
time before	15:20	15:53	16:39	19:28	17:23	18:05	18:45	20:10
injection time	15:22	15:56	16:43	19:31	17:27	18:08	18:51	20:13
s. after	7,05	4,92	3,7	0,6	1,2	0,6	1,50	2,44
time after	15:23	15:57	16:44	19:33	17:27	18:09	18:52	20:17
actual	12,84	6,59	8,61	5,47	7,77	7,01	5,35	3,82

Appendix No. 2:

The recorded data which were generated by PMOD software. Although we recorded five averaged of regions iBAT, heart, liver and brain we focused on evaluation of iBAT. The values of average voxels [kBq/cc] (cubic centimeter) The standardized uptake value (SUV) was calculated as SUV = VOI activity multiplied r [kBq/ml] by mouse weight w [g] divided by injected dose a‘ [kBq] (Figure 7). Id [kBq/cc] is actual dose per mouse.

- **^{18}F-FTHA – normal temperature**

Lfdiet

		cage: 4				Average	
		mouse 4	mouse 5	mouse 6	mouse 7	[kBg/cc]	St. Dev
Averaged	**iBAT**	119,589	145,3072	117,8212	124,1683	126,72142	12,67591
[kBq/cc]	**heart**	146,0669	124,6237	130,7721	143,5585	136,25529	10,24636
	liver	403,0668	757,0694	404,3022	448,4357	503,21853	170,5445
	brain	44,79803	56,98083	51,17054	54,1826	51,783001	5,226228
	id						
	[kBq/cc]	6350	7960	8290	5960		
	weight	26,3	26,6	25,4	24,9		
SUV	**iBAT**	0,495306	0,485574	0,360996	0,518757	0,4651582	0,070824
	abat						
	heart	0,60497	0,416456	0,400677	0,599766	0,5054672	0,112097
	liver	1,669395	2,529905	1,238755	1,873498	1,8278882	0,53762
	brain	0,185541	0,190413	0,156783	0,226367	0,1897762	0,028553

Hfdiet

		cage: 1			Average	
		mouse 4	mouse 5	mouse 6	[kBg/cc]	St. Dev
Averaged	**iBAT**	229,5581	56,75687	109,0134	131,7762	88,62096
[kBq/cc]	**heart**	890,6763	206,369	342,369	479,8048	362,2645
	liver	1455,023	212,9377	437,0202	701,6602	661,9815
	brain	140,8732	32,17059	63,1651	78,7363	55,99921
	id					
	[kBq/cc]	14100	5180	9780		
	weight	28,4	27,6	28,1		
SUV	**iBAT**	0,462372	0,302411	0,313219	0,359334	0,089397
	abat					
	heart	1,793986	1,099572	0,983698	1,292419	0,438217
	liver	2,930684	1,134572	1,255651	1,773636	1,003861
	brain	0,283745	0,171411	0,181487	0,212214	0,062152

- **^{18}F-FDG normal temperature**

Lfdiet

		cage: 3			cage: 4				Average	
		mouse 1	mouse 2	mouse 3	mouse 4	mouse 5	mouse 6	mouse 7	[kBg/cc]	St. Dev
Averaged	**iBAT**	1159,216	803,7235	515,5674	376,6522	238,56398	539,6462	373,8831	572,4647	313,9372
[kBq/cc]	**aBAT**	560,5228	497,2093	282,9894	131,8571	157,98715	252,7531	211,1067	299,2036	166,1438
	heart	415,2832	231,3512	188,8871	328,0644	238,17791	455,6076	250,7502	301,1602	101,315
	liver	99,18561	121,693	122,1213	52,2749	47,362336	63,75119	40,51155	78,12855	35,38676
	brain	355,9072	282,5877	196,7598	172,3463	161,94788	160,4015	130,8913	208,6917	80,79419
	id									
	[kBq/cc]	9540	9660	7070	6530	5170	6490	5010		
	weight	25,1	26,4	27	27,2	27,1	24,4	25,9		
SUV	**iBAT**	3,04993	2,196512	1,968928	1,568903	1,2504998	2,02887	1,932849	2,405123	0,569895
	abat	1,474751	1,358833	1,080723	0,549236	0,8281338	0,950258	1,09135	1,304769	0,202501
	heart	1,092621	0,632264	0,721351	1,366516	1,2484761	1,712916	1,296293	0,815412	0,244168
	liver	0,26096	0,332577	0,466375	0,217745	0,2482629	0,239681	0,209431	0,353304	0,104264
	brain	0,936402	0,772289	0,751416	0,71789	0,8488951	0,60305	0,676663	0,820036	0,101315

Hfdiet

		cage: 2			cage: 1				Average	
		mouse 1	mouse 2	mouse 3	mouse 4	mouse 5	mouse 6	mouse 7	[kBg/cc]	St. Dev
Averaged	**iBAT**	931,5184	514,281	382,4199	602,1765	397,0003	366,2616	466,1786	522,8337	198,6061
[kBq/cc]	**aBAT**		473,24	308,2549	419,0344	323,6233	258,1508	369,2459	358,5916	78,42961
	heart	332,3098	595,1438	361,9839	587,8087	599,114	492,44	978,0935	563,842	213,641
	liver	596,8618	151,1492	84,08429	111,2574	118,9206	52,01381	80,31047	170,6568	190,5998
	brain	56,67752	444,1721	340,6139	462,0688	433,0887	268,4056	438,9117	349,1341	146,6375
	id									
	[kBq/cc]	13580	11510	8860	12920	11070	11290	10140		
	weight	26	27,7	26,8	28,9	27,2	30	23,5		
SUV	**iBAT**	1,783467	1,23767	1,156755	1,346974	0,975466	0,973237	1,080394	1,221995	0,282276
	abat		1,138901	0,932419	0,937314	0,795172	0,685963	0,855747	0,763645	0,364721
	heart	0,636234	1,432275	1,09494	1,314835	1,472078	1,308521	2,266785	1,36081	0,489698
	liver	1,14274	0,363756	0,254341	0,248865	0,292199	0,138212	0,186124	0,375177	0,346078
	brain	0,108514	1,068946	1,030299	1,033575	1,064139	0,713212	1,017202	0,86227	0,354828

- **^{18}F-FTHA – normal temperature**

Lfdiet

		cage: 4 mouse 4	mouse 5	mouse 6	mouse 7	Average [kBg/cc]	St. Dev.
Averaged [kBq/cc]	**iBAT**	98,29023	98,29023	62,58807	99,768	89,7341	18,11078
	aBAT						
	heart	332,3098	332,3098	49,94881	198,2372	228,2014	134,5969
	liver	596,8618	596,8618	302,06	455,3626	487,7866	140,642
	brain	56,67752	56,67752	21,66073	38,06322	43,2697	16,86806
	id						
	[kBq/cc]	5750	3340	2800	5120		
	weight	26,2	26,7	24,4	25,4		
SUV	**iBAT**	0,447862	0,785733	0,54541	0,494943	0,568487	0,150208
	aBAT						
	heart	1,514177	2,656488	0,435268	0,983442	1,3973438	0,94798
	liver	2,719614	4,771321	2,632237	2,259025	3,0955494	1,134896
	brain	0,258252	0,453081	0,188758	0,188829	0,27223	0,124934

Hfdiet

		cage: 1 mouse 4	mouse 5	mouse 6	mouse 7	Average [kBg/cc]	St. Dev.
Averaged [kBq/cc]	**iBAT**	74,05845	132,1673	135,4684	141,082	120,6942	31,30742
	aBAT						
	heart	218,1933	168,8673	702,9084	265,9899	338,9897	245,8314
	liver	407,2567	181,0275	778,3893	925,758	573,1079	340,4586
	brain	32,56326	23,48968	53,44224	47,15807	39,16332	13,62629
	id						
	[kBq/cc]	4180	4140	9030	5610		
	weight	28,7	26,3	29,6	27,6		
SUV	**iBAT**	0,508487	0,839613	0,44406	0,694093	0,621564	0,179907
	aBAT						
	heart	1,498121	1,072756	2,304107	1,308613	1,545899	0,534581
	liver	2,796236	1,150006	2,551531	4,554532	2,763076	1,397278
	brain	0,22358	0,149222	0,175182	0,232008	0,194998	0,039475

- **^{18}F-FDG – cold exposure**

		Lfdiet					
		cage: 4				Average	
		mouse 4	mouse 5	mouse 6	mouse 7	[kBg/cc]	St.Dev
Averaged	**iBAT**	1001,384	996,0889591	829,5306	760,7195	896,9307	120,8843
[kBq/cc]	**aBAT**	355,8323	404,5216034	268,0078	294,891	330,8132	61,35633
	heart	337,5763	646,9224778	247,9095	411,1015	410,8774	170,9278
	liver	40,78508	86,60267017	38,20113	61,89909	56,87199	22,48388
	brain	126,207	174,4985082	102,4859	168,2618	142,8633	34,41723
	id						
	[kBq/cc]	6530	8900	4990	6940		
	weight	21,8	22,8	24,2	21,3		
SUV	**iBAT**	3,343058	2,551778457	4,022974	2,334773	3,063146	0,772797
	aBAT	1,187924	1,036302534	1,299757	0,905069	1,107263	0,172702
	heart	1,126978	1,65728455	1,202287	1,261738	1,312072	0,236656
	liver	0,136158	0,221858526	0,185264	0,189978	0,183315	0,035391
	brain	0,421334	0,447029886	0,497026	0,516423	0,470453	0,043896

		Hfdiet					
		cage: 1				Average	
		mouse 1	mouse 2	mouse 3	mouse 4	[kBg/cc]	St.Dev
Averaged	**iBAT**	863,991	644,584	558,1575	585,2154	662,987	138,7791
[kBq/cc]	**aBAT**	407,8789	311,5822	281,2785	303,46	326,0499	56,03597
	heart	720,9943	642,0625	474,1642	403,7007	560,2304	146,5725
	liver	89,60235	67,17047	52,84526	52,29689	65,47874	17,49454
	brain	288,0539	258,231	189,467	159,9202	223,918	59,36719
	id						
	[kBq/cc]	12370	9810	8230	7860		
	weight	24,8	22	23,1	23		
SUV	**iBAT**	1,732173	1,44555	1,566639	1,712462	1,614206	0,134509
	aBAT	0,817736	0,698757	0,789494	0,887987	0,798494	0,078332
	heart	1,445486	1,439896	1,330886	1,181312	1,349395	0,123852
	liver	0,179639	0,150637	0,148326	0,153032	0,157909	0,014614
	brain	0,577505	0,579111	0,531797	0,46796	0,539093	0,05225

- **^{18}F-FTHA – cold exposure II group**

Hfdiet

		cage: 2			cage: 1				Average	
		mouse 5	mouse 6	mouse 7	mouse 1	mouse 2	mouse 3	mouse 4	[kBg/cc]	St. Dev.
Averaged [kBq/cc]	**iBAT**	673,6494	522,4547	428,9876	157,7983	191,9599	44,92884	182,3351	314,5877	229,1464
	aBAT									
	heart	1172,407	995,0928	669,3271	313,8938	223,4251	45,84701	219,7325	519,9607	431,8689
	liver	2378,647	1696,147	2250,791	913,418	448,69	128,3445	796,6264	1230,381	884,1968
	brain	243,413	182,9797	198,3296	67,60158	44,83288	10,53861	52,84885	114,3635	91,28446
	id									
	[kBq/cc]	40170	16560	15530	9570	5340	1760	6340		
	weight	22,5	20,9	23,1	25,4	23,5	22,3	22,3		
SUV	**iBAT**	0,377324	0,659378	0,638095	0,418817	0,844767	0,569269	0,641336	0,592712	0,157893
	aBAT									
	heart	0,656688	1,255884	0,995586	0,833114	0,983238	0,580902	0,772876	0,868327	0,229984
	liver	1,332327	2,140669	3,347925	2,424328	1,974572	1,626184	2,802014	2,235431	0,690187
	brain	0,13634	0,230935	0,295004	0,179423	0,197298	0,133529	0,185888	0,194061	0,056031

Lfdiet

		cage: 3			cage: 4				Average	
		mouse 1	mouse 2	mouse 3	mouse 4	mouse 5	mouse 6	mouse 7	[kBg/cc]	St.Dev.
Averaged [kBq/cc]	**iBAT**	123,7422	267,8885	357,7955	441,6352	251,5454788	264,8874	263,8856	281,6257	98,33657
	aBAT									
	heart	91,58986	212,3939	170,4	543,6494	249,4076427	358,0442	307,7727	276,1797	146,7924
	liver	434,677	1025,49	994,8465	1184,619	758,7372742	949,325	807,7426	879,3482	241,5889
	brain	51,43711	86,37866	78,80663	137,9752	74,65963959	82,04662	78,46429	84,25259	26,22833
	id									
	[kBq/cc]	5690	10340	8570	20180	9600	11700	10020		
	weight	21,8	20,8	22,5	22,3	22,8	24	21,1		
SUV	**iBAT**	0,474091	0,538886	0,93937	0,488031	0,597420512	0,543359	0,555687	0,590978	0,159115
	aBAT									
	heart	0,350907	0,427253	0,447375	0,600762	0,592343151	0,73445	0,648104	0,543028	0,137181
	liver	1,66537	2,062882	2,611907	1,309068	1,802001026	1,947333	1,700935	1,871357	0,40483
	brain	0,19707	0,17376	0,206902	0,15247	0,177316644	0,168301	0,165229	0,177293	0,01881

- **^{18}F-FDG – warm exposure**

Lfdiet

		cage: 4 mouse 4	mouse 5	mouse 6	mouse 7	Average [kBg/cc]	St.Dev
Averaged [kBq/cc]	**iBAT**	1001,384	996,0889591	829,5306	760,7195	896,9307	120,8843
	aBAT	355,8323	404,5216034	268,0078	294,891	330,8132	61,35633
	heart	337,5763	646,9224778	247,9095	411,1015	410,8774	170,9278
	liver	40,78508	86,60267017	38,20113	61,89909	56,87199	22,48388
	brain	126,207	174,4985082	102,4859	168,2618	142,8633	34,41723
	id						
	[kBq/cc]	6530	8900	4990	6940		
	weight	21,8	22,8	24,2	21,3		
SUV	**iBAT**	3,343058	2,551778457	4,022974	2,334773	3,063146	0,772797
	aBAT	1,187924	1,036302534	1,299757	0,905069	1,107263	0,172702
	heart	1,126978	1,65728455	1,202287	1,261738	1,312072	0,236656
	liver	0,136158	0,221858526	0,185264	0,189978	0,183315	0,035391
	brain	0,421334	0,447029886	0,497026	0,516423	0,470453	0,043896

Hfdiet

		cage: 1 mouse 1	mouse 2	mouse 3	mouse 4	Average [kBg/cc]	St.Dev
Averaged [kBq/cc]	**iBAT**	863,991	644,584	558,1575	585,2154	662,987	138,7791
	aBAT	407,8789	311,5822	281,2785	303,46	326,0499	56,03597
	heart	720,9943	642,0625	474,1642	403,7007	560,2304	146,5725
	liver	89,60235	67,17047	52,84526	52,29689	65,47874	17,49454
	brain	288,0539	258,231	189,467	159,9202	223,918	59,36719
	id						
	[kBq/cc]	12370	9810	8230	7860		
	weight	24,8	22	23,1	23		
SUV	**iBAT**	1,732173	1,44555	1,566639	1,712462	1,614206	0,134509
	aBAT	0,817736	0,698757	0,789494	0,887987	0,798494	0,078332
	heart	1,445486	1,439896	1,330886	1,181312	1,349395	0,123852
	liver	0,179639	0,150637	0,148326	0,153032	0,157909	0,014614
	brain	0,577505	0,579111	0,531797	0,46796	0,539093	0,05225

- **^{18}F-FTHA – warm exposure II group**

Hfdiet

		cage: 2			cage: 1				Average	
		mouse 5	mouse 6	mouse 7	mouse 1	mouse 2	mouse 3	mouse 4	[kBg/cc]	St. Dev.
Averaged [kBq/cc]	**iBAT**	673,6494	522,4547	428,9876	157,7983	191,9599	44,92884	182,3351	314,5877	229,1464
	aBAT									
	heart	1172,407	995,0928	669,3271	313,8938	223,4251	45,84701	219,7325	519,9607	431,8689
	liver	2378,647	1696,147	2250,791	913,418	448,69	128,3445	796,6264	1230,381	884,1968
	brain	243,413	182,9797	198,3296	67,60158	44,83288	10,53861	52,84885	114,3635	91,28446
	id									
	[kBq/cc]	40170	16560	15530	9570	5340	1760	6340		
	weight	22,5	20,9	23,1	25,4	23,5	22,3	22,3		
SUV	**iBAT**	0,377324	0,659378	0,638095	0,418817	0,844767	0,569269	0,641336	0,592712	0,157893
	aBAT									
	heart	0,656688	1,255884	0,995586	0,833114	0,983238	0,580902	0,772876	0,868327	0,229984
	liver	1,332327	2,140669	3,347925	2,424328	1,974572	1,626184	2,802014	2,235431	0,690187
	brain	0,13634	0,230935	0,295004	0,179423	0,197298	0,133529	0,185888	0,194061	0,056031

Lfdiet

		cage: 3			cage: 4				Average	
		mouse 1	mouse 2	mouse 3	mouse 4	mouse 5	mouse 6	mouse 7	[kBg/cc]	St.Dev.
Averaged [kBq/cc]	**iBAT**	123,7422	267,8885	357,7955	441,6352	251,5454788	264,8874	263,8856	281,6257	98,33657
	aBAT									
	heart	91,58986	212,3939	170,4	543,6494	249,4076427	358,0442	307,7727	276,1797	146,7924
	liver	434,677	1025,49	994,8465	1184,619	758,7372742	949,325	807,7426	879,3482	241,5889
	brain	51,43711	86,37866	78,80663	137,9752	74,65963959	82,04662	78,46429	84,25259	26,22833
	id									
	[kBq/cc]	5690	10340	8570	20180	9600	11700	10020		
	weight	21,8	20,8	22,5	22,3	22,8	24	21,1		
SUV	**iBAT**	0,474091	0,538886	0,93937	0,488031	0,597420512	0,543359	0,555687	0,590978	0,159115
	aBAT									
	heart	0,350907	0,427253	0,447375	0,600762	0,592343151	0,73445	0,648104	0,543028	0,137181
	liver	1,66537	2,062882	2,611907	1,309068	1,802001026	1,947333	1,700935	1,871357	0,40483
	brain	0,19707	0,17376	0,206902	0,15247	0,177316644	0,168301	0,165229	0,177293	0,01881

Appendix No. 3:

The record of average volumes of iBAT per mouse which were generated by PMOD™ software. Data are presented as means ± SEM. [ccm] – cubic centimetre.

18F-FDG	room temperature			0 week			
	HFdiet						
	cage: 1			cage2			
	mouse 1	mouse 2	mouse 3	mouse 4	mouse 5	mouse 6	mouse 7
iBAT	0,451651	0,460601	0,274451082	0,455230816	1,277987427	0,977881136	0,630640855

18F-FDG	room temperature			0 week			
	Lfdiet						
	cage:3			cage:4			
	mouse 1	mouse 2	mouse 3	mouse 4	mouse 5	mouse 6	mouse 7
iBAT	0,869294	0,973108	1,0632	1,008309	0,656296	0,751757	0,706413

18F-FDG	room temperature			2 week			
	HFdiet						
	cage: 1				cage 2		
	mouse 4	mouse 5	mouse 6	mouse 7	mouse 1	mouse 2	mouse 3
iBAT	0,913445	0,788749	0,687320969		0,454634183		0,494011947

18F-FDG	room temperature			2 week			
	Lfdiet						
	cage:3				cage:4		
	mouse 1	mouse 2	mouse 3		mouse 4	mouse 5	mouse 6	mouse 7
iBAT	1,097208	0,801874	0,458214		0,527423	0,520264	0,443895	0,773833

18F-FTHA	room temperature			0 week				
	HFdiet				Lfdiet			
	cage: 1				cage 4			
	mouse 4	mouse 5	mouse 6	mouse 7	mouse 4	mouse 5	mouse 6	mouse 7
iBAT	0,075176	0,112167	0,168250446		0,096057879	0,11574676	0,206434944	0,103217472

18F-FTHA	room temperature			2 week				
	HFdiet				Lfdiet			
	cage: 1				cage 4			
	mouse 4	mouse 5	mouse 6	mouse 7	mouse 4	mouse 5	mouse 6	mouse 7
iBAT	0,075772	0,053697	0,05489	0,095461	0,11515	0,10978	0,061453	0,047134

18F-FTHA	cold temperature		2 week				
	HFdiet						
	cage: 1				cage 2		
	mouse 1	mouse 2	mouse 3	mouse 4	mouse 1	mouse 2	mouse 3
iBAT	0,119327	0,147368	0,125292885	0,061453177	0,205241678	0,175410039	0,200468616

18F-FTHA	cold temperature			2 week			
	LFdiet						
	cage: 3			cage 4			
	mouse 1	mouse 2	mouse 3	mouse 4	mouse 5	mouse 6	mouse 7
iBAT	0,112167	0,292947		0,097848	0,139015		0,110974

18F-FDG	cold temperature			0 week
	HFdiet			
	cage: 1			
	mouse 1	mouse 2	mouse 3	mouse 4
iBAT	0,908075	0,778009	0,684934438	0,708203117

18F-FDG	cold temperature			0 week
	Lfdiet			
	cage:4			
	mouse 4	mouse 5	mouse 6	mouse 7
iBAT	0,452248	0,58828	0,412273	0,770253

18F-FTHA	cold temperature			0 week			
	HFdiet						
	cage: 1				cage 2		
	mouse 1	mouse 2	mouse 3	mouse 4	mouse 1	mouse 2	mouse 3
iBAT	0,119327	0,147368	0,125292885	0,061453177	0,205241678	0,175410039	0,200468616

18F-FTHA	cold temperature			0 week				
	LFdiet							
	cage: 3				cage 4			
	mouse 4	mouse 5	mouse 6	mouse 7	mouse 1	mouse 2	mouse 3	mouse 4
iBAT	D	0,045941	0,033411	0,050714	0,084722	0,060857	0,071596	0,065033

18F-FDG	warm temperature			0 week			
	HFdiet						
	cage: 1			cage 2			
	mouse 1	mouse 2	mouse 3	mouse 4	mouse 5	mouse 6	mouse 7
iBAT	0,394971	0,815	0,665245556	0,202258514	0,299509659	0,197485452	0,161687485

18F-FDG	warm temperature			0 week			
	LFdiet						
	cage: 3			cage 4			
	mouse 1	mouse 2	mouse 3	mouse 4	mouse 5	mouse 6	mouse 7
iBAT	0,223141	0,690304		0,346644	0,549499	0,546516	0,050395

18F-FTHA	warm temperature			0 week	
	HFdiet				
	cage: 1			cage 2	
	mouse 1	mouse 2	mouse 3	mouse 4	mouse 5
iBAT	0,029832	0,092478	0,038781131	0,054890216	

18F-FTHA	warm temperature			0 week			
	LFdiet						
	cage: 3				cage 4		
	mouse 1	mouse 2	mouse 3	mouse 4	mouse 5	mouse 6	mouse 7
iBAT	0,025059	0,03594	0,04788		0,044151	0,0531	0,038184

18F-FDG	warm temperature			2 week		
	HFdiet					
	cage: 1			cage 2		
	mouse 1	mouse 2	mouse 3	mouse 4	mouse 5	mouse 6
iBAT	0,187939	0,080545	0,171830242	0,097251144	0,08770502	0,121116456

18F-FDG	warm temperature			2 week			
	Lldiet						
	cage: 3			cage 4			
	mouse 1	mouse 2	mouse 3	mouse 4	mouse 5	mouse 6	mouse 7
iBAT	0,22851	0,226124	0,130663	0,098444	0,073982	0,073982	0,116343

18F-FTHA	warm temperature			2 week		
	HFdiet					
	cage: 1			cage 2		
	mouse 1	mouse 2	mouse 3	mouse 4	mouse 5	mouse 6
iBAT		0,065033	0,058470013	0,095461246	0,111570331	0,053696951

18F-FTHA	warm temperature			2 week			
	LFdiet						
	cage: 3				cage 4		
	mouse 1	mouse 2	mouse 3	mouse 4	mouse 5	mouse 6	mouse 7
iBAT	0,292947	0,150948	0,050117	0,12589		0,110974	

Appendix No. 4:

The overall statistic evaluation of SUV values of iBAT. These comparison were performed by GraphPad Prism 7. For statistical evaluation of differences between each group was used a parametric T-test. The Normality tests confirmed that our data are parametric. The Anova test were subsequently set up.

RT0 (room temperature, week 0), FDG (flourogeoxyglucose), LFD (low fat diet), HFD (high fat diet), FTHA (fluoro-thia-heptadecanoic acid), RT2 (room temperature, week 2), CT0 (cold temperature, week 0), CT2 (cold temperature, week 2), WT0 (warm temperature, week 0). WT2. (warm temperature, week 2).

Tukey's multiple comparisons test	Mean Diff,	Significant?	Summary	Adjusted P Value
RT0_FDG_LFD vs. RT0_FDG_HFD	1,226	No	Ns	0,1617
RT0_FDG_LFD vs. RT0_FTHA_LFD	2,145	Yes	***	0,0005
RT0_FDG_LFD vs. RT0_FTHA_HFD	2,27	Yes	***	0,0009
RT0_FDG_LFD vs. RT2_FDG_HFD	1,395	Yes	*	0,0473
RT0_FDG_LFD vs. RT2_FDG_LFD	0,5623	No	Ns	0,9976
RT0_FDG_LFD vs. RT2_FTHA_HFD	2,008	Yes	**	0,0017
RT0_FDG_LFD vs. RT2_FTHA_LFD	2,055	Yes	**	0,0011
RT0_FDG_LFD vs. CT0_FDG_HFD	0,9846	No	ns	0,7947
RT0_FDG_LFD vs. CT0_FDG_LFD	-0,5499	No	ns	0,9998
RT0_FDG_LFD vs. CT0_FTHA_HFD	2,04	Yes	****	<0,0001
RT0_FDG_LFD vs. CT0_FTHA_LFD	2,027	Yes	***	0,0002
RT0_FDG_LFD vs. CT2_FDG_HFD	0,9356	No	ns	0,7834
RT0_FDG_LFD vs. CT2_FDG_LFD	-0,458	No	ns	0,9999
RT0_FDG_LFD vs. CT2_FTHA_HFD	2,215	Yes	***	0,0003
RT0_FDG_LFD vs. CT2_FTHA_LFD	2,215	Yes	***	0,0003

Tukey's multiple comparisons test	Mean Diff,	Significant?	Summary	Adjusted P Value
RT0_FDG_LFD vs. WT0_FDG_HFD	1,25	No	ns	0,1375
RT0_FDG_LFD vs. WT0_FDG_LFD	0,03489	No	ns	>0,9999
RT0_FDG_LFD vs. WR0_FTHA_HFD	2,225	Yes	***	0,0002
RT0_FDG_LFD vs. WT0_FTHA_LFD	2,159	Yes	**	0,0022
RT0_FDG_LFD vs. WR2_FDG_HFD	1,451	Yes	*	0,0444
RT0_FDG_LFD vs. WT2_FDG_LFD	0,3085	No	ns	>0,9999
RT0_FDG_LFD vs. WT2_FTHA_HFD	2,207	Yes	**	0,0015
RT0_FDG_LFD vs. WT2_FTHA_LFD	2,212	Yes	**	0,0014
RT0_FDG_HFD vs. RT0_FTHA_LFD	0,9193	No	ns	0,7957
RT0_FDG_HFD vs. RT0_FTHA_HFD	1,044	No	ns	0,7493
RT0_FDG_HFD vs. RT2_FDG_HFD	0,1687	No	ns	>0,9999
RT0_FDG_HFD vs. RT2_FDG_LFD	-0,6636	No	ns	0,949
RT0_FDG_HFD vs. RT2_FTHA_HFD	0,782	No	ns	0,9465
RT0_FDG_HFD vs. RT2_FTHA_LFD	0,8295	No	ns	0,908
RT0_FDG_HFD vs. CT0_FDG_HFD	-0,2413	No	ns	>0,9999
RT0_FDG_HFD vs. CT0_FDG_LFD	-1,776	Yes	**	0,0044
RT0_FDG_HFD vs. CT0_FTHA_HFD	0,8139	No	ns	0,7393
RT0_FDG_HFD vs. CT0_FTHA_LFD	0,8013	No	ns	0,8202
RT0_FDG_HFD vs. CT2_FDG_HFD	-0,2903	No	ns	>0,9999
RT0_FDG_HFD vs. CT2_FDG_LFD	-1,684	Yes	***	0,0007
RT0_FDG_HFD vs. CT2_FTHA_HFD	0,9893	No	ns	0,6778
RT0_FDG_HFD vs. CT2_FTHA_LFD	0,989	No	ns	0,6783
RT0_FDG_HFD vs. WT0_FDG_HFD	0,02454	No	ns	>0,9999
RT0_FDG_HFD vs. WT0_FDG_LFD	-1,191	No	ns	0,1347
RT0_FDG_HFD vs. WR0_FTHA_HFD	0,9989	No	ns	0,6602
RT0_FDG_HFD vs. WT0_FTHA_LFD	0,9329	No	ns	0,8898

Tukey's multiple comparisons test	Mean Diff,	Significant?	Summary	Adjusted P Value
RT0_FDG_HFD vs. WR2_FDG_HFD	0,2247	No	ns	>0,9999
RT0_FDG_HFD vs. WT2_FDG_LFD	-0,9174	No	ns	0,5155
RT0_FDG_HFD vs. WT2_FTHA_HFD	0,9812	No	ns	0,8362
RT0_FDG_HFD vs. WT2_FTHA_LFD	0,9857	No	ns	0,8306
RT0_FTHA_LFD vs. RT0_FTHA_HFD	0,1248	No	ns	>0,9999
RT0_FTHA_LFD vs. RT2_FDG_HFD	-0,7506	No	ns	0,9646
RT0_FTHA_LFD vs. RT2_FDG_LFD	-1,583	Yes	*	0,0235
RT0_FTHA_LFD vs. RT2_FTHA_HFD	-0,1374	No	ns	>0,9999
RT0_FTHA_LFD vs. RT2_FTHA_LFD	-0,08985	No	ns	>0,9999
RT0_FTHA_LFD vs. CT0_FDG_HFD	-1,161	No	ns	0,6044
RT0_FTHA_LFD vs. CT0_FDG_LFD	-2,695	Yes	****	<0,0001
RT0_FTHA_LFD vs. CT0_FTHA_HFD	-0,1055	No	ns	>0,9999
RT0_FTHA_LFD vs. CT0_FTHA_LFD	-0,1181	No	ns	>0,9999
RT0_FTHA_LFD vs. CT2_FDG_HFD	-1,21	No	ns	0,4156
RT0_FTHA_LFD vs. CT2_FDG_LFD	-2,603	Yes	****	<0,0001
RT0_FTHA_LFD vs. CT2_FTHA_HFD	0,06993	No	ns	>0,9999
RT0_FTHA_LFD vs. CT2_FTHA_LFD	0,06967	No	ns	>0,9999
RT0_FTHA_LFD vs. WT0_FDG_HFD	-0,8948	No	ns	0,8314
RT0_FTHA_LFD vs. WT0_FDG_LFD	-2,11	Yes	***	0,0003
RT0_FTHA_LFD vs. WR0_FTHA_HFD	0,07957	No	ns	>0,9999
RT0_FTHA_LFD vs. WT0_FTHA_LFD	0,01358	No	ns	>0,9999
RT0_FTHA_LFD vs. WR2_FDG_HFD	-0,6947	No	ns	0,9894
RT0_FTHA_LFD vs. WT2_FDG_LFD	-1,837	Yes	**	0,0025
RT0_FTHA_LFD vs. WT2_FTHA_HFD	0,06188	No	ns	>0,9999
RT0_FTHA_LFD vs. WT2_FTHA_LFD	0,06641	No	ns	>0,9999
RT0_FTHA_HFD vs. RT2_FDG_HFD	-0,8754	No	ns	0,9373

Tukey's multiple comparisons test	Mean Diff,	Significant?	Summary	Adjusted P Value
RT0_FTHA_HFD vs. RT2_FDG_LFD	-1,708	Yes	*	0,0303
RT0_FTHA_HFD vs. RT2_FTHA_HFD	-0,2622	No	ns	>0,9999
RT0_FTHA_HFD vs. RT2_FTHA_LFD	-0,2146	No	ns	>0,9999
RT0_FTHA_HFD vs. CT0_FDG_HFD	-1,285	No	ns	0,5549
RT0_FTHA_HFD vs. CT0_FDG_LFD	-2,82	Yes	****	<0,0001
RT0_FTHA_HFD vs. CT0_FTHA_HFD	-0,2303	No	ns	>0,9999
RT0_FTHA_HFD vs. CT0_FTHA_LFD	-0,2429	No	ns	>0,9999
RT0_FTHA_HFD vs. CT2_FDG_HFD	-1,334	No	ns	0,3893
RT0_FTHA_HFD vs. CT2_FDG_LFD	-2,728	Yes	****	<0,0001
RT0_FTHA_HFD vs. CT2_FTHA_HFD	-0,05485	No	ns	>0,9999
RT0_FTHA_HFD vs. CT2_FTHA_LFD	-0,05511	No	ns	>0,9999
RT0_FTHA_HFD vs. WT0_FDG_HFD	-1,02	No	ns	0,7853
RT0_FTHA_HFD vs. WT0_FDG_LFD	-2,235	Yes	***	0,0006
RT0_FTHA_HFD vs. WR0_FTHA_HFD	-0,04521	No	ns	>0,9999
RT0_FTHA_HFD vs. WT0_FTHA_LFD	-0,1112	No	ns	>0,9999
RT0_FTHA_HFD vs. WR2_FDG_HFD	-0,8194	No	ns	0,975
RT0_FTHA_HFD vs. WT2_FDG_LFD	-1,962	Yes	**	0,0042
RT0_FTHA_HFD vs. WT2_FTHA_HFD	-0,0629	No	ns	>0,9999
RT0_FTHA_HFD vs. WT2_FTHA_LFD	-0,05837	No	ns	>0,9999
RT2_FDG_HFD vs. RT2_FDG_LFD	-0,8324	No	ns	0,7016
RT2_FDG_HFD vs. RT2_FTHA_HFD	0,6132	No	ns	0,9969
RT2_FDG_HFD vs. RT2_FTHA_LFD	0,6607	No	ns	0,9918
RT2_FDG_HFD vs. CT0_FDG_HFD	-0,4101	No	ns	>0,9999
RT2_FDG_HFD vs. CT0_FDG_LFD	-1,945	Yes	***	0,0009
RT2_FDG_HFD vs. CT0_FTHA_HFD	0,6451	No	ns	0,9616
RT2_FDG_HFD vs. CT0_FTHA_LFD	0,6325	No	ns	0,9798

Tukey's multiple comparisons test	Mean Diff,	Significant?	Summary	Adjusted P Value
RT2_FDG_HFD vs. CT2_FDG_HFD	-0,459	No	ns	0,9999
RT2_FDG_HFD vs. CT2_FDG_LFD	-1,853	Yes	****	<0,0001
RT2_FDG_HFD vs. CT2_FTHA_HFD	0,8205	No	ns	0,9164
RT2_FDG_HFD vs. CT2_FTHA_LFD	0,8203	No	ns	0,9166
RT2_FDG_HFD vs. WT0_FDG_HFD	-0,1442	No	ns	>0,9999
RT2_FDG_HFD vs. WT0_FDG_LFD	-1,36	Yes	*	0,0352
RT2_FDG_HFD vs. WR0_FTHA_HFD	0,8302	No	ns	0,9074
RT2_FDG_HFD vs. WT0_FTHA_LFD	0,7642	No	ns	0,9851
RT2_FDG_HFD vs. WR2_FDG_HFD	0,05593	No	ns	>0,9999
RT2_FDG_HFD vs. WT2_FDG_LFD	-1,086	No	ns	0,203
RT2_FDG_HFD vs. WT2_FTHA_HFD	0,8125	No	ns	0,9704
RT2_FDG_HFD vs. WT2_FTHA_LFD	0,817	No	ns	0,9686
RT2_FDG_LFD vs. RT2_FTHA_HFD	1,446	No	ns	0,0669
RT2_FDG_LFD vs. RT2_FTHA_LFD	1,493	Yes	*	0,0473
RT2_FDG_LFD vs. CT0_FDG_HFD	0,4223	No	ns	>0,9999
RT2_FDG_LFD vs. CT0_FDG_LFD	-1,112	No	ns	0,4478
RT2_FDG_LFD vs. CT0_FTHA_HFD	1,477	Yes	**	0,0066
RT2_FDG_LFD vs. CT0_FTHA_LFD	1,465	Yes	*	0,0134
RT2_FDG_LFD vs. CT2_FDG_HFD	0,3733	No	ns	>0,9999
RT2_FDG_LFD vs. CT2_FDG_LFD	-1,02	No	ns	0,3064
RT2_FDG_LFD vs. CT2_FTHA_HFD	1,653	Yes	*	0,0132
RT2_FDG_LFD vs. CT2_FTHA_LFD	1,653	Yes	*	0,0132
RT2_FDG_LFD vs. WT0_FDG_HFD	0,6882	No	ns	0,9281
RT2_FDG_LFD vs. WT0_FDG_LFD	-0,5274	No	ns	0,998
RT2_FDG_LFD vs. WR0_FTHA_HFD	1,663	Yes	*	0,0121
RT2_FDG_LFD vs. WT0_FTHA_LFD	1,597	No	ns	0,0648

Tukey's multiple comparisons test	Mean Diff,	Significant?	Summary	Adjusted P Value
RT2_FDG_LFD vs. WR2_FDG_HFD	0,8883	No	ns	0,6568
RT2_FDG_LFD vs. WT2_FDG_LFD	-0,2538	No	ns	>0,9999
RT2_FDG_LFD vs. WT2_FTHA_HFD	1,645	Yes	*	0,047
RT2_FDG_LFD vs. WT2_FTHA_LFD	1,649	Yes	*	0,0455
RT2_FTHA_HFD vs. RT2_FTHA_LFD	0,04753	No	ns	>0,9999
RT2_FTHA_HFD vs. CT0_FDG_HFD	-1,023	No	ns	0,814
RT2_FTHA_HFD vs. CT0_FDG_LFD	-2,558	Yes	****	<0,0001
RT2_FTHA_HFD vs. CT0_FTHA_HFD	0,0319	No	ns	>0,9999
RT2_FTHA_HFD vs. CT0_FTHA_LFD	0,0193	No	ns	>0,9999
RT2_FTHA_HFD vs. CT2_FDG_HFD	-1,072	No	ns	0,6548
RT2_FTHA_HFD vs. CT2_FDG_LFD	-2,466	Yes	****	<0,0001
RT2_FTHA_HFD vs. CT2_FTHA_HFD	0,2073	No	ns	>0,9999
RT2_FTHA_HFD vs. CT2_FTHA_LFD	0,207	No	ns	>0,9999
RT2_FTHA_HFD vs. WT0_FDG_HFD	-0,7574	No	ns	0,9611
RT2_FTHA_HFD vs. WT0_FDG_LFD	-1,973	Yes	**	0,0012
RT2_FTHA_HFD vs. WR0_FTHA_HFD	0,2169	No	ns	>0,9999
RT2_FTHA_HFD vs. WT0_FTHA_LFD	0,151	No	ns	>0,9999
RT2_FTHA_HFD vs. WR2_FDG_HFD	-0,5573	No	ns	0,9995
RT2_FTHA_HFD vs. WT2_FDG_LFD	-1,699	Yes	**	0,0088
RT2_FTHA_HFD vs. WT2_FTHA_HFD	0,1993	No	ns	>0,9999
RT2_FTHA_HFD vs. WT2_FTHA_LFD	0,2038	No	ns	>0,9999
RT2_FTHA_LFD vs. CT0_FDG_HFD	-1,071	No	ns	0,748
RT2_FTHA_LFD vs. CT0_FDG_LFD	-2,605	Yes	****	<0,0001
RT2_FTHA_LFD vs. CT0_FTHA_HFD	-0,01563	No	ns	>0,9999
RT2_FTHA_LFD vs. CT0_FTHA_LFD	-0,02823	No	ns	>0,9999
RT2_FTHA_LFD vs. CT2_FDG_HFD	-1,12	No	ns	0,5713

Tukey's multiple comparisons test	Mean Diff,	Significant?	Summary	Adjusted P Value
RT2_FTHA_LFD vs. CT2_FDG_LFD	-2,513	Yes	****	<0,0001
RT2_FTHA_LFD vs. CT2_FTHA_HFD	0,1598	No	ns	>0,9999
RT2_FTHA_LFD vs. CT2_FTHA_LFD	0,1595	No	ns	>0,9999
RT2_FTHA_LFD vs. WT0_FDG_HFD	-0,8049	No	ns	0,9297
RT2_FTHA_LFD vs. WT0_FDG_LFD	-2,021	Yes	***	0,0008
RT2_FTHA_LFD vs. WR0_FTHA_HFD	0,1694	No	ns	>0,9999
RT2_FTHA_LFD vs. WT0_FTHA_LFD	0,1034	No	ns	>0,9999
RT2_FTHA_LFD vs. WR2_FDG_HFD	-0,6048	No	ns	0,9983
RT2_FTHA_LFD vs. WT2_FDG_LFD	-1,747	Yes	**	0,0058
RT2_FTHA_LFD vs. WT2_FTHA_HFD	0,1517	No	ns	>0,9999
RT2_FTHA_LFD vs. WT2_FTHA_LFD	0,1563	No	ns	>0,9999
CT0_FDG_HFD vs. CT0_FDG_LFD	-1,535	No	ns	0,1197
CT0_FDG_HFD vs. CT0_FTHA_HFD	1,055	No	ns	0,5544
CT0_FDG_HFD vs. CT0_FTHA_LFD	1,043	No	ns	0,6353
CT0_FDG_HFD vs. CT2_FDG_HFD	-0,04898	No	ns	>0,9999
CT0_FDG_HFD vs. CT2_FDG_LFD	-1,443	No	ns	0,0684
CT0_FDG_HFD vs. CT2_FTHA_HFD	1,231	No	ns	0,4873
CT0_FDG_HFD vs. CT2_FTHA_LFD	1,23	No	ns	0,4877
CT0_FDG_HFD vs. WT0_FDG_HFD	0,2659	No	ns	>0,9999
CT0_FDG_HFD vs. WT0_FDG_LFD	-0,9497	No	ns	0,7913
CT0_FDG_HFD vs. WR0_FTHA_HFD	1,24	No	ns	0,4715
CT0_FDG_HFD vs. WT0_FTHA_LFD	1,174	No	ns	0,7233
CT0_FDG_HFD vs. WR2_FDG_HFD	0,466	No	ns	>0,9999
CT0_FDG_HFD vs. WT2_FDG_LFD	-0,6761	No	ns	0,9891
CT0_FDG_HFD vs. WT2_FTHA_HFD	1,223	No	ns	0,6522
CT0_FDG_HFD vs. WT2_FTHA_LFD	1,227	No	ns	0,6453

Tukey's multiple comparisons test	Mean Diff,	Significant?	Summary	Adjusted P Value
CT0_FDG_LFD vs. CT0_FTHA_HFD	2,59	Yes	****	<0,0001
CT0_FDG_LFD vs. CT0_FTHA_LFD	2,577	Yes	****	<0,0001
CT0_FDG_LFD vs. CT2_FDG_HFD	1,486	No	ns	0,0997
CT0_FDG_LFD vs. CT2_FDG_LFD	0,09193	No	ns	>0,9999
CT0_FDG_LFD vs. CT2_FTHA_HFD	2,765	Yes	****	<0,0001
CT0_FDG_LFD vs. CT2_FTHA_LFD	2,765	Yes	****	<0,0001
CT0_FDG_LFD vs. WT0_FDG_HFD	1,8	Yes	**	0,0036
CT0_FDG_LFD vs. WT0_FDG_LFD	0,5848	No	ns	0,9989
CT0_FDG_LFD vs. WR0_FTHA_HFD	2,775	Yes	****	<0,0001
CT0_FDG_LFD vs. WT0_FTHA_LFD	2,709	Yes	****	<0,0001
CT0_FDG_LFD vs. WR2_FDG_HFD	2,001	Yes	***	0,0009
CT0_FDG_LFD vs. WT2_FDG_LFD	0,8585	No	ns	0,8774
CT0_FDG_LFD vs. WT2_FTHA_HFD	2,757	Yes	****	<0,0001
CT0_FDG_LFD vs. WT2_FTHA_LFD	2,762	Yes	****	<0,0001
CT0_FTHA_HFD vs. CT0_FTHA_LFD	-0,0126	No	ns	>0,9999
CT0_FTHA_HFD vs. CT2_FDG_HFD	-1,104	No	ns	0,3288
CT0_FTHA_HFD vs. CT2_FDG_LFD	-2,498	Yes	****	<0,0001
CT0_FTHA_HFD vs. CT2_FTHA_HFD	0,1754	No	ns	>0,9999
CT0_FTHA_HFD vs. CT2_FTHA_LFD	0,1751	No	ns	>0,9999
CT0_FTHA_HFD vs. WT0_FDG_HFD	-0,7893	No	ns	0,7861
CT0_FTHA_HFD vs. WT0_FDG_LFD	-2,005	Yes	****	<0,0001
CT0_FTHA_HFD vs. WR0_FTHA_HFD	0,185	No	ns	>0,9999
CT0_FTHA_HFD vs. WT0_FTHA_LFD	0,1191	No	ns	>0,9999
CT0_FTHA_HFD vs. WR2_FDG_HFD	-0,5892	No	ns	0,9913
CT0_FTHA_HFD vs. WT2_FDG_LFD	-1,731	Yes	***	0,0004
CT0_FTHA_HFD vs. WT2_FTHA_HFD	0,1674	No	ns	>0,9999

Tukey's multiple comparisons test	Mean Diff,	Significant?	Summary	Adjusted P Value
CT0_FTHA_HFD vs. WT2_FTHA_LFD	0,1719	No	ns	>0,9999
CT0_FTHA_LFD vs. CT2_FDG_HFD	-1,092	No	ns	0,4162
CT0_FTHA_LFD vs. CT2_FDG_LFD	-2,485	Yes	****	<0,0001
CT0_FTHA_LFD vs. CT2_FTHA_HFD	0,188	No	ns	>0,9999
CT0_FTHA_LFD vs. CT2_FTHA_LFD	0,1877	No	ns	>0,9999
CT0_FTHA_LFD vs. WT0_FDG_HFD	-0,7767	No	ns	0,8574
CT0_FTHA_LFD vs. WT0_FDG_LFD	-1,992	Yes	****	<0,0001
CT0_FTHA_LFD vs. WR0_FTHA_HFD	0,1976	No	ns	>0,9999
CT0_FTHA_LFD vs. WT0_FTHA_LFD	0,1317	No	ns	>0,9999
CT0_FTHA_LFD vs. WR2_FDG_HFD	-0,5766	No	ns	0,9959
CT0_FTHA_LFD vs. WT2_FDG_LFD	-1,719	Yes	***	0,001
CT0_FTHA_LFD vs. WT2_FTHA_HFD	0,18	No	ns	>0,9999
CT0_FTHA_LFD vs. WT2_FTHA_LFD	0,1845	No	ns	>0,9999
CT2_FDG_HFD vs. CT2_FDG_LFD	-1,394	Yes	*	0,0477
CT2_FDG_HFD vs. CT2_FTHA_HFD	1,28	No	ns	0,3077
CT2_FDG_HFD vs. CT2_FTHA_LFD	1,279	No	ns	0,308
CT2_FDG_HFD vs. WT0_FDG_HFD	0,3148	No	ns	>0,9999
CT2_FDG_HFD vs. WT0_FDG_LFD	-0,9007	No	ns	0,7754
CT2_FDG_HFD vs. WR0_FTHA_HFD	1,289	No	ns	0,2942
CT2_FDG_HFD vs. WT0_FTHA_LFD	1,223	No	ns	0,5645
CT2_FDG_HFD vs. WR2_FDG_HFD	0,515	No	ns	0,9996
CT2_FDG_HFD vs. WT2_FDG_LFD	-0,6271	No	ns	0,99
CT2_FDG_HFD vs. WT2_FTHA_HFD	1,272	No	ns	0,4864
CT2_FDG_HFD vs. WT2_FTHA_LFD	1,276	No	ns	0,4792
CT2_FDG_LFD vs. CT2_FTHA_HFD	2,673	Yes	****	<0,0001
CT2_FDG_LFD vs. CT2_FTHA_LFD	2,673	Yes	****	<0,0001

Tukey's multiple comparisons test	Mean Diff,	Significant?	Summary	Adjusted P Value
CT2_FDG_LFD vs. WT0_FDG_HFD	1,708	Yes	***	0,0005
CT2_FDG_LFD vs. WT0_FDG_LFD	0,4929	No	ns	0,9992
CT2_FDG_LFD vs. WR0_FTHA_HFD	2,683	Yes	****	<0,0001
CT2_FDG_LFD vs. WT0_FTHA_LFD	2,617	Yes	****	<0,0001
CT2_FDG_LFD vs. WR2_FDG_HFD	1,909	Yes	***	0,0001
CT2_FDG_LFD vs. WT2_FDG_LFD	0,7665	No	ns	0,8257
CT2_FDG_LFD vs. WT2_FTHA_HFD	2,665	Yes	****	<0,0001
CT2_FDG_LFD vs. WT2_FTHA_LFD	2,67	Yes	****	<0,0001
CT2_FTHA_HFD vs. CT2_FTHA_LFD	-0,00026	No	ns	>0,9999
CT2_FTHA_HFD vs. WT0_FDG_HFD	-0,9647	No	ns	0,7215
CT2_FTHA_HFD vs. WT0_FDG_LFD	-2,18	Yes	***	0,0002
CT2_FTHA_HFD vs. WR0_FTHA_HFD	0,009636	No	ns	>0,9999
CT2_FTHA_HFD vs. WT0_FTHA_LFD	-0,05635	No	ns	>0,9999
CT2_FTHA_HFD vs. WR2_FDG_HFD	-0,7646	No	ns	0,9684
CT2_FTHA_HFD vs. WT2_FDG_LFD	-1,907	Yes	**	0,0013
CT2_FTHA_HFD vs. WT2_FTHA_HFD	-0,00806	No	ns	>0,9999
CT2_FTHA_HFD vs. WT2_FTHA_LFD	-0,00352	No	ns	>0,9999
CT2_FTHA_LFD vs. WT0_FDG_HFD	-0,9645	No	ns	0,7219
CT2_FTHA_LFD vs. WT0_FDG_LFD	-2,18	Yes	***	0,0002
CT2_FTHA_LFD vs. WR0_FTHA_HFD	0,0099	No	ns	>0,9999
CT2_FTHA_LFD vs. WT0_FTHA_LFD	-0,05609	No	ns	>0,9999
CT2_FTHA_LFD vs. WR2_FDG_HFD	-0,7643	No	ns	0,9685
CT2_FTHA_LFD vs. WT2_FDG_LFD	-1,906	Yes	**	0,0013
CT2_FTHA_LFD vs. WT2_FTHA_HFD	-0,00779	No	ns	>0,9999
CT2_FTHA_LFD vs. WT2_FTHA_LFD	-0,00326	No	ns	>0,9999
WT0_FDG_HFD vs. WT0_FDG_LFD	-1,216	No	ns	0,1127

Tukey's multiple comparisons test	Mean Diff,	Significant?	Summary	Adjusted P Value
WT0_FDG_HFD vs. WR0_FTHA_HFD	0,9744	No	ns	0,7046
WT0_FDG_HFD vs. WT0_FTHA_LFD	0,9084	No	ns	0,9122
WT0_FDG_HFD vs. WR2_FDG_HFD	0,2001	No	ns	>0,9999
WT0_FDG_HFD vs. WT2_FDG_LFD	-0,9419	No	ns	0,4619
WT0_FDG_HFD vs. WT2_FTHA_HFD	0,9567	No	ns	0,865
WT0_FDG_HFD vs. WT2_FTHA_LFD	0,9612	No	ns	0,8599
WT0_FDG_LFD vs. WR0_FTHA_HFD	2,19	Yes	***	0,0001
WT0_FDG_LFD vs. WT0_FTHA_LFD	2,124	Yes	**	0,0016
WT0_FDG_LFD vs. WR2_FDG_HFD	1,416	Yes	*	0,0338
WT0_FDG_LFD vs. WT2_FDG_LFD	0,2737	No	ns	>0,9999
WT0_FDG_LFD vs. WT2_FTHA_HFD	2,172	Yes	**	0,0011
WT0_FDG_LFD vs. WT2_FTHA_LFD	2,177	Yes	**	0,001
WR0_FTHA_HFD vs. WT0_FTHA_LFD	-0,06599	No	ns	>0,9999
WR0_FTHA_HFD vs. WR2_FDG_HFD	-0,7742	No	ns	0,964
WR0_FTHA_HFD vs. WT2_FDG_LFD	-1,916	Yes	**	0,0012
WR0_FTHA_HFD vs. WT2_FTHA_HFD	-0,01769	No	ns	>0,9999
WR0_FTHA_HFD vs. WT2_FTHA_LFD	-0,01316	No	ns	>0,9999
WT0_FTHA_LFD vs. WR2_FDG_HFD	-0,7082	No	ns	0,9957
WT0_FTHA_LFD vs. WT2_FDG_LFD	-1,85	Yes	*	0,0104
WT0_FTHA_LFD vs. WT2_FTHA_HFD	0,04829	No	ns	>0,9999
WT0_FTHA_LFD vs. WT2_FTHA_LFD	0,05283	No	ns	>0,9999
WR2_FDG_HFD vs. WT2_FDG_LFD	-1,142	No	ns	0,1883
WR2_FDG_HFD vs. WT2_FTHA_HFD	0,7565	No	ns	0,9901
WR2_FDG_HFD vs. WT2_FTHA_LFD	0,7611	No	ns	0,9894
WT2_FDG_LFD vs. WT2_FTHA_HFD	1,899	Yes	**	0,0071
WT2_FDG_LFD vs. WT2_FTHA_LFD	1,903	Yes	**	0,0068

Tukey's multiple comparisons test	Mean Diff,	Significant?	Summary	Adjusted P Value
WT2_FTHA_HFD vs. WT2_FTHA_LFD	0,004534	No	ns	>0,9999